ADDIS ABABA UNIVERSITY

ADDIS ABABA INSTITUTE OF TECHNOLOGY

SCHOOL OF MULTI-DISCIPLINARY ENGINEERING

CENTER FOR MATERIALS ENGINEERING

Citrate Stabilized Magnetic Nanoparticles (Fe_3O_4) for the Removal of Pb^{2+} Ions in Wastewater.

A Thesis Submitted to the Center for Materials Engineering, Addis Ababa Institute of Technology, for the Partial Fulfillment of the Requirements for the Degree of Masters of Science in Materials Engineering

By

Solomon Mamuye Ladanke

Adsvisor

Tesfaye Refera Soreta (Ph.D.)

Addis Ababa University

Addis Ababa, Ethiopia

Jun, 2022

ADDIS ABABA UNIVERSITY

ADDIS ABABA INSTITUTE OF TECHNOLOGY

SCHOOL OF MULTI-DISCIPLINARY ENGINEERING

CENTER FOR MATERIALS ENGINEERING

Citrate Stabilized Magnetic Nanoparticles (Fe_3O_4) for the Removal of Pb^{2+} Ions in Wastewater.

A thesis submitted to the Research and Graduate School of Addis Ababa University, Addis Ababa Institute of Technology, Center for Materials Engineering in partial fulfillment of the requirements for the attainment of the Degree of Masters of Science in Material Engineering.

By: Solomon Mamuye Ladanke

Approved by the Examining Committee:

Tesfaye Refera Soreta (Ph.D.)		
(Main Advisor)	signature	date
Sintayehu Nibret Tiruneh (Ph.D.)		
(Internal Examiner)	signature	date
Shimelis Kebede Kassahun (Ph.D.)		
(External Examiner)	signature	date

Declaration

I, SOLOMON MAMUYE, declare that this thesis entitled "Citrate stabilized magnetic nanoparticles for the removal of Pb^{2+} ions in wastewater" has not been submitted in any form for another degree, diploma or an award at any university or other institution of the tertiary education. Whenever contributions of others are involved, every effort is made to indicate this clearly, with due reference to the literature and discussions. Information taken from published and unpublished work of others has been acknowledged in the text, and a list of references is given. The research work was undertaken with the guidance of my advisor, Tesfaye Refera Soreta (Ph.D.) Associate Professor in Addis Ababa University, Addis Ababa Institute of Technology, School of Multi-Disciplinary Engineering, Center for Materials Engineering.

Acknowledgements

First of all, I humbly acknowledge my heartfelt gratitude to the almighty God, the most gracious, benevolent, and merciful whose benediction has been guiding me to the light throughout the days and always.

I wish to express my deepest gratitude and sincere thanks to my honorable advisor, Tesfaye Refera Soreta (Ph.D.) Associate Professor, for providing me with an opportunity to work under his guidance. His kind attention, care, and continuous encouragement have been a source of inspiration throughout the research.

I want to express my deep gratitude to my co-advisor, Dawit Gemechu (Ph.D.), for his advice and insightful comments.

My thanks also extend to all staff members of the Center of Materials Engineering and laboratory technicians of AAiT, especially Mr. Hinetsaselasie, for being their untried support during the lab work.

Finally, special thanks are due to my immediate family, my daughters, Blen Solomon, and Ruth Solomon, who provided an endless source of motivation, ultimate love, and blissful inspiration and were always with me throughout my life.

Abstract

Water contaminations by heavy metals are a major environmental problem due to their acute toxicity and their accumulation in food chains. One of such toxic heavy metals is Pb^{2+} ions. In this study the synthesis of bare magnetite nanoparticles (B-MNPs), and citric acid coated magnetite nanoparticles (Cit-MNPs) to remove heavy metal Pb^{2+} ions from wastewater is reported. The Fe_3O_4 MNPs were synthesized using standard co-precipitation methods. The as such prepared MNPs were characterized by AAS, XRD, FTIR, BET, and Zetasizer. Citric acid was used as surface coating and functionalization of MNPs to increase the selectivity of the magnetic MNPs towards Pb^{2+} ions. Using a permanent magnet, the Cit-MNPs were easily separated from the mixture after adsorption of Pb^{2+} ions. The adsorption of Pb^{2+} ions from synthetic wastewater was tested using a batch experiment to assess the feasibility of the prepared MNPs. The main operational parameters namely pH, adsorbent mass, initial Pb^{2+} ions concentration, and contact time were investigated to understand the optimal experimental conditions for removal of Pb^{2+} ions. The adsorption efficiency was highly pH-dependent. The maximum removal efficiencies of Pb^{2+} ions on Cit-MNPs and B-MNPs were over 96.1% and 83.3%, using adsorbent dose: 0.1 g/L , at pH: 5, contact time: 60 minutes, initial metal ions concentration: 50 mg/L, shaker speed: 200 rpm, and temperature: normal, respectively. The sorption of Pb^{2+} ions onto nanoadsorbents obeyed the Freundlich adsorption isotherm model. The maximum adsorption capacity achieved by Cit-MNPs is about 200 mg/g, which is higher than B-MNPs, i.e., 111.1 mg/g. A kinetic study confirms more the pseudo-second-order model with R^2 = 0.99. The first-order rate constant of K_1 and second-order rate constant of K_2 were found to be, $K_1 = 1.1x10^{-2}$ $minute^{-1}$, $K_2 = 1.3x10^{-2}$ $minute^{-1}$for B-MNPs and $K_1 = 1.9x10^{-2}$ $minute^{-1}$, $K_2 = 1.4x10^{-2}$ $minute^{-1}$ for Cit-MNPs, respectively. This result confirmed that the synthesized MNPs nanoadsorbents are considered the most promising sorbent with high efficiency and more feasible to remove Pb^{2+}, a heavy metal ions from synthetic wastewater.

Keywords: Magnetite nanoparticles, Citric acid, Wastewater, Lead ions, Adsorption.

Table of Contents

List of Tables

List of Figures

List of Abbreviations

AAS:	Atomic absorption spectroscopy
AC:	Activated carbon
b:	Langmuir constant
B-MNPs:	Bare magnetite nanoparticles
CA:	Citric acid
CAC:	Commercial activated carbon
C_e:	Equilibrium ion concentration
C_i:	Initial ion concentration
Cit-MNPs:	Citric acid coated magnetite nanoparticles
CNTs:	Carbon nanotubes
D:	Crystalline size (nm)
DNA:	Deoxyribonucleic acid
EPA:	Environmental protection agency
FAC:	Fibrous activated carbon
FCC:	Face cubic centered
FTIR:	Furior transform infrared
GAC:	Granular activated carbon
IQ:	Intelligence quotient
JCPDS:	Joint committee on powder diffraction standards
K_1:	Rate constant of Pseudo-first-order kinetics (min^{-1})
$K_{2:}$	Rate constant of pseudo-second-order kinetics ($g.mg^{-1}.min^{-1}$)
$K_{F:}$	Freundlich constant
MF:	Microfiltration
MNPs:	Magnetite nanoparticles
N:	Intensity of adsorption
NF:	Nanofiltration
NPs:	Nanoparticles
nZVI:	Nano-zero valent iron
PAC:	Powder Activated Carbon
PEG:	Polyethylene glycol

ppm:	part per million
q_e:	Equilibrium adsorption capacity
q_m:	maximum adsorption capacity
R:	Correlation coefficient
RO:	Reverse osmosis
rpm:	Round per minute
UF:	Ultrafiltration
WHO:	World health organization
XRD:	X-ray diffraction

CHAPTER ONE

1 Introduction

1.1 Background of the study

Nowadays, nanotechnology has persuaded meaningful scientific advancement in research and new technology. Nanotechnology deals with the understanding of small objects which can be used across all scientific areas such as chemistry, biology, physics, and also applied to material science and engineering. As understood from the name, nano refers to a billionth (10^{-9}) of a unit. Nanomaterials size range varies from 1-100 nm [1]. Nano size particles are unique because they increase surface area to volume ratio, and also, their physical, chemical, and biological properties are distinct from their bulk material. So in recent years, many researchers have been investigating the structure, properties, and function of nanomaterials.

MNPs have attracted much attention due to their low toxicity, biocompatibility, super-paramagnetic properties, large surface area to volume ratio, and a good reactive surface [2]. The extreme reactivity of iron makes it difficult to study and problematic for applications. However, strong magnetic and catalytic properties have diverted attention toward iron's potential [1, 2]. Preparation methods, size, shape, crystallization, and quality of the iron oxide NPs highly affect these behaviors [3].

Iron oxides are prevalent, inexpensive, and the most widely used bio-compatible materials, which are necessary for many biological and geological processes. Magnetite (Fe_3O_4), maghemite (γ-Fe_2O_3), and hematite (α-Fe_2O_3) are the three most common forms of iron oxides in nature, which are also very important in the field of scientific research [4].

Water is one of the basic needs of living organisms. Water quality is changed day to day due to population growth and environmental changes. In the rural and urban areas, ground and surface water are the primary source of drinking water; however, the availability of potable water is still a significant concern [6]. Toxic heavy metals are substantial contributors to water pollution because of their high aqueous solubility, non-biodegradability, and potential toxicity even at trace levels [8]. Among different heavy

metals, lead metals (Pb) are perhaps the most toxic and cause several detrimental health problems such as cancer, anaemia, malfunctioning of vital organs and the central nervous system. Human activities like mining, smelting, electroplating, tanning, textile, paint industries, etc., are considerable sources of Pb pollution. The Pb^{2+} ions containing aqueous effluent contaminate the surface as well as ground water. Pb^{2+} ions concentration above prescribed limits in water affects humans as well as the environment health. The WHO and USEPA maximum admissible limit of Pb^{2+} ions is 0.1 g/L in drinking water. Therefore, avoidance of Pb^{2+} ions from an aqueous system has been a primary concern for the scientific community [9].

MNPs known for their excellent magnetic properties and easy production methods, are suitable adsorbents for eliminating contaminants from wastewater. But still, agglomeration and oxidation in the air during synthesis are the main challenges. Surface coating has been employed in past years as a way of solving difficulties encountered to the aggregation of MNPs using them as adsorbents. Surface coating and functionalization stabilizes not only the magnetic core from oxidation and agglomeration but also improves the adsorption capability of the materials. At present, many researchers and scientists recommend that surface functionalization of the magnetic cores with chelating ligands' enhance its effectiveness in the removal of contaminants [7, 10].

Surface functionalization gives the material a new surface chemical property such as solubility, reactivity, stability, melting point, and electronic structure different from that of the original material [11]. Surface functionalization makes size distribution homogenous in size and has a good shape distribution, and controls its stability in aqueous solutions. Acid surface-functionalized MNPs have been reported to remove heavy metals from aqueous solutions [12].

In the recent past, different approaches, namely coagulation, flocculation, ion-exchange, electrodialysis, precipitation, ultrafiltration, etc., have been applied to sequestration of Pb^{2+} ions from water and wastewater [13]. However, poor adeptness, sludge generation, restricted flexibility, high energy consumption, and complex experimental setup are the drawbacks of the technologies mentioned above. Apart from these physical techniques,

the adsorptive separation of heavy metals using nanosized adsorbents has received considerable attention from the scientific community [14].

1.2 Statement of the problem

Among different metallic nanomaterials, Fe_3O_4 NPs have attracted considerable attention due to their distinct physicochemical properties. Nowadays, the synthesis of nanoparticles through co-precipitation has proven to be a better method as it is effective, easily scaled up, and environment friendly for large scale synthesis [15].

The main drawbacks of synthesized MNPs are the agglomeration (aggregation), broad size distribution, and poor Zeta potential values. Synthesized Fe_3O_4 NPs also lack good colloidal stability and have inadequate repulsive forces to prevent agglomeration. To conquer these problems, the Fe_3O_4 NPs essentially stable, and their size distribution must be decreased by coating their surfaces with appropriate materials. Various surface modifier agents are used like polyethylene glycol (PEG), SiO_2, ionic liquids, etc...[14]. Still, this study focuses on surface functionalization with citric acid (CA) to modify the size, stability from aggregation, and enhancing the adsorbing capacity of the MNPs. CA has a strong metal ions chelating property, which has been highly investigated to improve the dissolution of heavy metal ions. The negative surface charge of MNPs given by CA prevented agglomeration in wastewater suspension [14, 15]. The intention of this study is to elaborate whether CA affects the adsorption of Pb^{2+} ions on MNPs, and how this will occur in the adsorption performance of MNPs. Batch adsorption experiments including isotherm equilibrium, kinetics, regeneration and reusability measurements will also conducted.

Due to increased industrialization and poor waste management in Ethiopia, the rate of water pollution that is majorly caused by discharging from industries is growing. In addition, contaminated liquid wastewaters, which include heavy metals such as Pb^{2+} ions, inorganic and organic chemicals, and pathogens/microbes, are the primary concern in Ethiopia. For this reason, a more effective, lower-cost, and robust NPs synthesis method to detoxify liquid wastewater is needed. The magnetic Fe_3O_4 NPs have been utilized in many applications, including wastewater treatment.

1.3 Justification

This study aimed at the synthesis of bare magnetite nanoparticles (B-Fe_3O_4) and citric acid coated (Cit-Fe_3O_4) NPs for removal of heavy metal Pb^{2+} ions from polluted wastewater. The adsorption of CA onto the surface of Fe_3O_4 nanoparticles could result in a highly negative surface charge formation. This negative charge is due to the presence of uncoordinated negatively charged carboxylate groups on the surface of Fe_3O_4 nanoparticles [11]. Hence, in this work, we proposed that there will be reasonably high electrostatic interactions between the surface of the negatively charged Cit-MNP and positively charged Pb^{2+} ions in the wastewater through the adsorption process.

1.4 Objective of the study

1.4.1 General objectives

The main objective of this study is to synthesize iron oxide (B-Fe_3O_4) nanoadsorbents and surface modification of iron oxide nanoadsorbents with citric acid (Cit-Fe_3O_4) to remove toxic Pb^{2+} ions from liquid waste through adsorption.

1.4.2 Specific objectives

The specific objectives of this study are:

- To synthesize bare magnetite (B-Fe_3O_4) NPs and surface modified with citric acid magnetite (Cit-Fe_3O_4) NPs using the co-precipitation method.
- To examine the synthesized (B-Fe_3O_4) and (Cit-Fe_3O_4) NPs using X-ray diffraction (XRD), BET, FTIR spectrometer, and Zetasizer.
- To evaluate the adsorbing efficiency and capacity of bare (B-Fe_3O_4) and modified (Cit-Fe_3O_4) nanoadsorbents to remove toxic Pb^{2+} ions from wastewater at different pH, adsorbent dose, contact time, and initial concentrations of Pb^{2+} ions.
- To investigate the adsorption isotherms and adsorption kinetics model of the as prepared samples.

1.5 Significance of the study

This work is expected to have its contribution to the synthesis of Fe_3O_4 NPs and its surface modification using citric acid. It is believed that this research will bring positive impacts on increasing a technology transfer and encourage Ethiopian researchers to

explore various additional applications of MNPs. Releasing toxic heavy metals from industrial, agricultural, and domestic wastewaters has become a threat to the ecosystems in Ethiopia. So, to handle this growing threat, the synthesis of magnetite nanomaterial and its investigation is very necessary. Nanosize, materials are successful adsorbents for eliminating toxic heavy metals from contaminated wastewater due to their larger surface area, improved active sites, and the functional groups that exist on their surface [16].

This study demonstrates magnetite nanoparticles used as adsorbent for toxic heavy metals from contaminated wastewater via a batch adsorption process. Environmental pollution caused by this wastewater would be minimized. The potential of the low-cost adsorbent from MNPs to remove heavy metal Pb^{2+} ions from wastewater will significantly help in reducing the number of people affected by lung cancer, nerve disorders, and mental retardation [17].

CHAPTER TWO

2 Literature Review

2.1 General overview

Presently, sustainable initiatives that are used in a greener way to improve and protect our global environments are the focal concerns in many kinds of research. Synthesis of nanomaterials in advance with low cost and environmentally friendly approaches remains a scientific challenge. MNPs are used in various applications such as catalysis, electronics, biology, biomedical, material science, physics, and environmental remediation [18]. This study is concerned with the synthesis of Fe_3O_4 nanoparticles modified with citric acid for the removal of lead ions in wastewater. The followings research findings are reviewed related to this study line.

2.2 The heavy metal pollutants that affect the environment

Heavy metals are metallic elements with a relatively higher density than water, and their atomic density is greater than 4 g/cm^3. Heavy metals such as lead, arsenic, nickel, chromium, mercury, cadmium, selenium, zinc, and copper are common heavy metal elements. These heavy metals can exist in trace quantities in humans and other mammals, causing substantial health problems [19].

Heavy metals are harmful to the environment and are a serious concern. The industrialization and urbanization is increasing that causes the heavy metals to be contaminating the environment, and it is a threat to human health [20]. In addition, heavy metals possess a major environmental problem to living organisms and their habitats because of their non-biodegradability, bioaccumulation, ecological instability, and bio-toxicity characteristics [5]. Therefore, due to the rising degrees of wastewater disposal with toxic heavy metals from factories daily, the environmental issue is getting a more significant concern.

High concentrations of heavy metals are disrupting the natural ecosystems and impacting the human bodies acutely and permanently via the food chain. Nondegradable heavy metals can also accumulate on the surface sediment for a long time through the food chain, causing various diseases and complications in the human body. In addition, the

heavy metals released into the water system may negatively affect water qualities such as pH of water, water temperature, surface sediments, bioturbation, etc. [21].

The existence of heavy metals in the biological system affects the cellular organelles and some other enzymes involved in the metabolism. The metal ions interact with the cell components such as DNA and nuclear protein, causing DNA damage and conformational alteration that may lead to cell cycle modulations, carcinogenesis, or apoptosis [22]. Various studies from the laboratory test indicated that reactive oxygen species (ROS) production and oxidative stresses play a critical role in the toxicity and carcinogenicity of metals such as arsenic (As), cadmium (Cd), chromium(Cr), lead(Pb), and mercury (Hg) [21]. Therefore, these five elements have a high degree of toxicity for public health.

Figure 1. Heavy metal contamination in the aquatic ecosystem [23].

2.2.1 Sources of lead metal

Lead (Pb) is heavy metal that naturally exists in the Earth's crust. In many parts of the world, wide usage of Pb element resulted in extensive environmental contaminations, human exposure, and considerable public health problems [17]

The main activities such as mining, smelting, Pb paints, Pb aviation fuels, etc., are sources of Pb metals that are caused for environmental contamination. More than three-quarters of global Pb consumption is for the production of lead-acid batteries in motor

vehicles. It is also applied in many other products such as pigments, paints, solders, stained glasses, lead crystal glass-wares, ammunition, ceramic glazes, jewellers, toys, and for some cosmetics and traditional medicines. In addition, drinking water delivered through lead pipes might contain Pb [17].

2.2.2 Health effects of lead

Pb metal exposure can have serious consequences for children′s health [17]. At greater levels of exposure, lead metal attacks the brain and the central nervous systems, causing coma, convulsions, and even death. The children exposed to severe lead metal poisoning may be left with intellectual disability and behavioral disorders. At lower levels of exposure, that might not cause noticeable symptoms, but through time, lead metal produces the spectrum of injury throughout multiple body systems. In particular, lead can influences children′s brain development, reducing intelligence quotient (IQ), the behavioral changes such as reduced attention, becoming against to social behavior, and low achiever in their education. Pb metal exposure also causes anemia, hypertension, renal impairments, immunotoxicity, and toxicity to the reproductive organs. The neurological and behavioral effects of Pb metal are believed to be irreversible [18].

2.3 Methods of removal of heavy metal pollutants

Several technologies have been employed to remove Pb from the wastewater stream, including chemical precipitation, ion exchange, membrane technology, electrochemical deposition, volatilization, oxidation-reduction, and mechanical filtration [25]. However, these techniques tend to be either ineffective or extremely expensive when removing heavy metal concentrations. Table 1, summarizes nine technologies recognized as being able to remove Pb from wastewater. Some factors should be considered before choosing a method to remove lead metal from an aqueous environment. It must not leave toxic residues that might release Pb in the future and must later be avoided by other methods. Large volumes of wastewater should be treated with low-cost treating materials [25]. Consequently, a preferable of the most appropriate treatment method for any given waste system, requires correct determinations of the volume and characteristics of the effluents.

Table 1. Some technologies for the treatment of lead (EPA, 2007) [24]

		Water	
Technology	Soil	Ground and surface water	Wastewater
Solidification/stabilization	✓		
Soil washing and acid extraction	✓		
Thermal treatment	✓		
Vitrification	✓		
Precipitation/Coprecipitation		✓	✓
Adsorption		✓	✓
Ion exchange		✓	✓
Membrane filtration			✓
Biological treatment			✓

2.3.1 The chemical precipitation process

Chemical precipitation is the conventional technology for the removal of toxic heavy metals, such as Hg, Pb, Zn, and Cu in large industrial plants. Heavy metals precipitated from the solution by adding alkali to raise the pH, as shown in Figure 3, and the settled sludge is then collected and dewatered before their ultimate disposal [26]. Precipitation technologies can reduce Pb concentrations to less than 2.0 μg/L. However, some methods, such as those based on activated carbon polishing, have been using multiple precipitation steps and other technologies as pre-treatments of reaching this level [24].

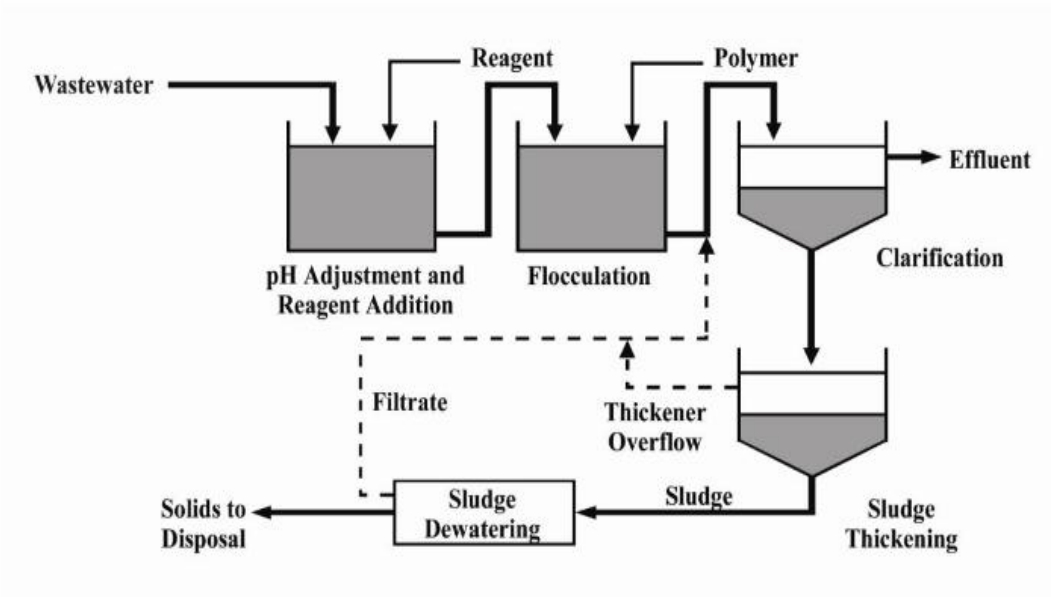

Figure 2. Schematic representation of precipitation system (EPA, 2007).

Since it is a very simple and highly efficient method for removing large quantities of Pb ions from the contaminated water, these methods are widely used in industries. However, the presence of the other contaminants, both dissolved, colloidal and suspended, might affect precipitation and therefore need to be removed through other processes [27]. The main problems related to precipitation processes are often followed by solid/ liquid separations process as a secondary step for, low density solids. The disposal of large amounts of sludge that usually contains high water is the greatest problem. The disposal of the unstable precipitates might cause secondary contaminates of water because there is sludge in which the metal ions can be returning to the aqueous environments. In addition to this, the polishing steps are required for most precipitation processes of metal ions to achieve lower residual levels of the processed wastewater [27].

2.3.2 Ion exchange process

The ion exchange method is used as non-consumptive technique for selective removal and recovery of heavy metals. The ions are removed from wastewater and concentrated on the exchange resin [28]. Then, the resins are regenerated. This method is a simple and highly effective technique for removing even trace amounts of impurities from the solutions. Such a process is used for removal of Pb(II), Cd(II), Zn(II), Hg(II), and Cr(III) from water solution and industrial wastewater. The ions exchange processes continue

until the solutions are treated and exhaust the resins exchange capacity. The exhausted resins must be regenerated by the other chemicals that can replace the ions captured in the ions exchange operation, thus converting the resins back to their original compositions to be reused in the next cycle [29]. Ion exchange has many problems in removing heavy metals, such as inadequate wettability, small surface areas, poor selectivity, slowest adsorption rate, and challenges in regeneration. In addition, the existence of suspended solids might affect the effectiveness of the ion exchange process. Moreover, during practice for wastewater treatment, ion exchange would not achieve the treatment goals, and pre-filtration is required to remove suspended solids that might mechanically block the resin′s bed [30].

2.3.3 Electrodialysis

Electrodialysis is an electrochemical reaction at which metal ions migrate through the ion selective semi-permeable membranes. Due to their attraction to the two electrically charged electrodes, removal of most charged dissolved ions is possible. The process applies direct current power to remove salts and other ionized species through cations and anions of the ion-selective membranes. Electrodialysis is very applicable for water treatments, removal of mineral salts, sulfates and nitrates from the water, and sea water. The shortcomings of these methods are the formation of metal hydroxides, which clog the membranes [30].

2.3.4 Membrane filtration

The membranes are a selective barrier, allowing some constituents to pass while clogging the passage of others. There are four types of membrane filtration methods, which are classified by their pore size: (1) reverse osmosis (RO), (2) microfiltration (MF), (3) nanofiltration (NF), and (4) ultrafiltration (UF) [31]. For Pb ion removal, the pre-treatment step should be used to form lead precipitates that can be more effectively removed by this technology. Then, membranes can reduce lead concentrations to less than 2.0 μg/L [24]. However, suspended solid, organic compounds, and other contaminants can cause membrane fouling during lead removals operation. To improve the separation of lead ions from aqueous waste, modern membranes are incorporated with functional materials or applied electric currents. Generally, membrane filtrations are not

used because they tend to produce larger volumes of residue than other lead treatment technologies [31].

2.3.5 Biological treatment

Despite the fact that, biological treatment remediation has been successfully applied to remove organic contaminants, it is not relevant to the elimination of lead ions from wastewater. It can, however, be used as the treatment by converting soluble ionic lead (Pb^{2+}) into elements or metallic lead (Pb^{0}) that is retained on the biomass where it is more easily removed from the wastewater by other technologies, such as adsorption or precipitation [32]. In this type of process, pre-treatment is expected to be applied to adjust the pH of the solution to have it in the optimal range at 6.5 to 7.5 using sodium hydroxide and phosphoric acid as optimization of the aerobic bio-treatment process [24].

The drawbacks associated with biological treatment are the high concentrations of Pb metal might be toxic to microorganisms used in biological treatment. Also, the presence of a sufficient amount of nutrients, such as yeast, and sucrose extracts, is crucial to the performance of the biological system. In addition, biological treatment is not suitable for in situ remediations because it requires extensive reactor setups. The other disadvantage is that the Pb metal concentration in the incoming wastewater must be adjusted. If a high amount flows, the Pb metals will overwhelm the bacteria and kill them [32].

2.3.6 Adsorption process

Among the wastewater treatment processes, the adsorption techniques are more advantageous. This is due to its high adsorption efficiency, facile handling, cost-effectiveness, recyclability, and operational simplicity [33]. Adsorption belongs to the surface phenomenon when adsorbates are adsorbed on a solid surface. The adsorbent material is the surface where adsorption occurs, and adsorbates are the metal ion adsorbed on the surface. Desorption is the reverse method of adsorption i.e. adsorbate substances are separated from the adsorbent surface to the liquid phase. The adsorption rate, to remove pollutants in wastewater, is determined by certain properties such as specific surface area, pore volume, porosity, interaction time, cation exchange capacity, and adsorbent dose [34].

The adsorptions of molecules can be represented as physical or chemical reactions:

$$A + B \leftrightarrow A.B \text{……..} (1)$$

Where A is the adsorbate (contaminant), B is the adsorbent, and A.B can be the adsorbed compounds.

Based on the interaction forces between adsorbate and adsorbent, adsorption is of two types, physical and chemical. Physical adsorption is accompanied by Vander Waals forces, static, and π interactions. Physical adsorption can be reversed and exothermic process with low adsorption heat. However, cross linking of adsorbates and adsorbent with strong chemical bonds leads to the chemisorption process [35].

Table 2. The difference between physisorption and chemisorption. [27]

Chemical adsorption	**Physical adsorption**
Chemical bonding is involved in the interaction between adsorbates and the surface of the adsorbents	Intermolecular forces are involved in the interaction between adsorbates and the surface of the adsorbents
Monolayer	Can be both monolayer or multi-layer
Highly specific	Nonspecific
Adsorption can occur over a wide temperature range	Occurs at low temperature
Bond are formed as a result of electron transfer	No transfer of electron
Adsorption may be slow and is irreversible	Adsorption is fast and interaction is reversible

2.4 Materials removal of lead by adsorption

There are many adsorbents that have already been researched, including activated carbon, fly ash, chitosan, clay, agricultural waste, and natural zeolites for removing lead from industrial effluent [36]. The production of advanced adsorbents with high efficiency for removal of Pb at lower concentrations is an essential task in the treatment of wastewater. The followings are some common adsorbents used to remove lead metal from wastewater.

2.4.1 Activated carbon

Activated carbon (AC) has been frequently used in industrial applications for Pb metal removal. AC is classified into four types based on their shape and size: powder (PAC), granular (GAC), fibrous (FAC), and clothe (CAC). Because of the different sources of raw materials, the degree of chemical activation, and the physicochemical characteristics, each type of AC has its specific application, inherent advantages, and drawbacks in wastewater treatment [37]. Although a substantial number of low-cost adsorbents from various materials have been investigated, the CAC is still the standard sorbent of Pb metal. Many researchers are continuing to formulate and investigate the use of AC for Pb metal removal. Various studies have been reported that the removal efficiency of Pb using GAC was more than 60% of total Pb at the range of Pb concentrations 1-30 μg/L at pH 7.0. The equilibrium time for the removal of lead metal was more than two hours and the GAC generally cannot be regenerated [37]. However, some results indicated that the regeneration processes are a little bit complicated. PAC is not widely used for the removal of lead metal as GAC because of low efficiency and the fact that it could not be regenerated for reuse. Due to intensive applications of AC, it has become an expensive material. The other disadvantage is that the activated carbon requires complexion agents to improve its removal performance of inorganic Pb metal. Recently, AC has ceased (stopped) to be attractive in small-scale industries because of cost-ineffectiveness reasons [38].

2.4.2 Fly ash

Fly ash is a solid industrial material generated from thermal power plants, such as coal combustion. Generally, fly ash is one of the most conventional and cheapest adsorbents for the removal of lead metal. However, the drawbacks of using fly ash were reported in the research works [39]. The report indicated that the adsorption capacity of fly ash is generally low, usually in between 2.5 up to 6 mg/g of Pb metal. Also, adsorption process requires a large amount of fly ash which cannot be replaced [39].

2.4.3 Peat moss

Peat moss, its originality from plants, mainly contains lignin and cellulose as the major components. Peat Moss is widely available and commonly used as a sorbent with

adsorption capabilities for lead metal removal. It is a porous material with a large surface area greater than 200 m^2/g and can be modified to improve its sorption capacity so that the high efficiency of binding or chelating heavy metals can be achieved [40]. Peat moss adsorbent materials are also relatively inexpensive sorbents and are commercially available with a lower average cost. Pb(II) metal′s peak adsorptions onto peat mosses were found at pH ranges between 3.5 and 6.5, and the maximum capacity obtained was 16.2 mg/g of Pb metal. The peat moss requires drying and chemical pre-treatment either with acid or alkali (base) to enhance its effective performance [40].

2.4.4 Clay minerals

The clay minerals such as micas, montmorillonite, and kaolinite have been widely used in lead metal removal. The adsorption capacities of clay minerals result from the net charge on the structures of very fine-grain silicate minerals. The other factors that contribute to the enhancement of adsorption capacities are the high surface area of clay minerals, about 800 m^2/g [42]. As can be compared and contrasted with the conventional adsorbents, the adsorption capacity of clay for Pb metal is very low, usually less than 1 mg/g at Pb metal concentrations of 1000 μg/L. However, the uptake and adsorbent capacity of clay minerals modified by thiol groups enhanced Pb(II) metal removal [41]. Clay minerals might require a high temperature to achieve their maximal adsorption, which increases the cost-effectiveness of this sorbent [41].

2.4.5 Zeolites

Zeolites are naturally occurring as micro-porous crystalline aluminosilicate consists of a frame-work of tetrahedral molecules linked to each other by oxygen atoms. Zeolites are generally cheap adsorbents related to their cost, and their price is very low relative to their quality. The surface area of zeolites is around 70 m^2/g. The mechanisms of adsorptions take place based on ion exchange, where cations bonded to negatively charged groups on the sorbent surface. Zeolites may not be regenerated for reuse [42].

Although the above mechanisms have been widely used for the removal of Pb metal from aqueous solutions, most of these materials suffer from inherent problems such as lower removal capacity, lower selectivity, longer equilibrium time, or mechanical and thermal

instability. Therefore, the formation of a new adsorbent should be managed by the following scenarios:

- The ideal adsorbent should have greater stability against coagulation, consist of insoluble porous materials, and have better active sites.
- It should be modified with organic or inorganic groups that interact with targeted pollutants.
- It should achieve fast adsorption with high efficient capacity and good reusability.

2.5 Application of advanced nanoparticles for removal of heavy metals

2.5.1 Application of non-magnetic NPs for environmental protection

Nanotechnology does not just concern manufacturing tiny structured materials but, more significantly, how these could be used to perform a specific task. Various studies reported that the environmental problems would be solved using nanomaterials. For example: NPs have been widely used for the treatment of contaminated soils, sediments, wastewater and solid wastes using many kinds of non-magnetic NPs [43]. Three major classes of the nanoparticles (NPs) are widely used for water and wastewater treatment, which includes metal containing (ceramic) NPs, Zeolites NPs, and carbonaceous NPs such as, carbon nanotube (CNTs) [44].

2.5.1.1 Carbon nanotubes

Due to their unique and exceptional properties, CNTs have attracted much research attention. CNTs have been applied for the removal of heavy metal ions such as lead Pb(II), Cu(II), Hg(II), and Cd(II). Its adsorbing capacity is three times higher than that of GAC. Although CNTs have indicated good potential in water purification technology, it is not widely used as adsorbent because it requires higher cost [44].

2.5.1.2 Nano-zero valent iron

nZVI have been used for degrading chlorinated organic compounds through the reduction because its reduction speed is faster than natural rates, however, it still can take the days. nZVI is usually applied for the degradation of chlorinated compound in water, such as trichloroethylene (TCE), or perchloroethylene (PCBs) [45]. There has also been some

kind of interest in using nZVI for the adsorption of heavy metals such as Pb(II), As(V), AS(III), and Cu(II). The nature of the low surface area and the presence of dissolved iron (Fe) during the adsorption processes at lower pH are disadvantages of using nZVI for the adsorption of heavy metals. Another drawback is its sensitivity to oxidation in air and aqueous media [44].

2.5.1.3 Titanium dioxide NPs

Titanium dioxide (TiO_2) NPs has been intensively and frequently used to remove organic contaminants from various media through oxidation and reduction. Chlorinated alkanes and benzene, dioxins, and polychlorinated biphenyls (PCBs) are some of the examples. TiO_2 NPs were not considered as a promising sorbent for the removal of heavy metals due to its carcinogen concern, its fate, and preparation cost. To increase its separation from treated water streams external magnetic field is used if TiO_2 NPs are coated with magnetic NPs [45].

2.5.1.4 Porous aluminum oxide NPs

Although porous aluminum oxide (Al_2O_3) NPs mostly is used as contaminant adsorbents for drinking water, it is not effective for the removal of Pb metals. In general, Al_2O_3 NPs do not have a favorable pore structure thus having lower adsorption capacities [46].

2.5.1.5 Mesoporous silica

Surface-modified mesoporous silicas are one of the most widely used adsorbents for removing of heavy metals due to large surface area and narrow pore distribution. Mercapto-mesoporous silica showed a higher affinity for the adsorption of Pb(II) metal from an aqueous solution using a batch method. In contrast, other divalent cations such as, Cu(II), Zn(II), Cr(VI) and Ni(II) present in wastewater are preferably adsorbed on amino group (-NH) functionalized mesoporous silica . Although the effectiveness of this nanosorbent has been sufficiently proved and increased, the present higher production costs are major drawbacks [47].

2.5.2 Application of magnetic NPs for water treatment

2.5.2.1 Magnetic iron oxide NPs

As shown in Figure 3, Fe_3O_4 is a magnetic iron oxide with a cubic inverse spinel crystal structure. Oxygen forming face centered cubic (FCC) closed packing. Iron Fe cations occupy interstitial tetrahedral sites and octahedral sites [5]. The unit cell is consisting of 56 atoms in which; 32 O^{2-} anions, 16 Fe^{3+}, and 8 Fe^{2+} cataions. Half of the Fe^{3+} ions occupy tetrahedral interstices and the remaining half of Fe^{3+} and all of the Fe^{2+} ions occupy the octahedral interstices. The size of O^{2-} anions is 1.26 Å, which are often larger than 0.75 Å of Fe^{2+} and 0.69 Å of Fe^{3+} cations. Thus, O^{2-} anions suited to the closed packing position and Fe cations occupy interstitial sites [81].

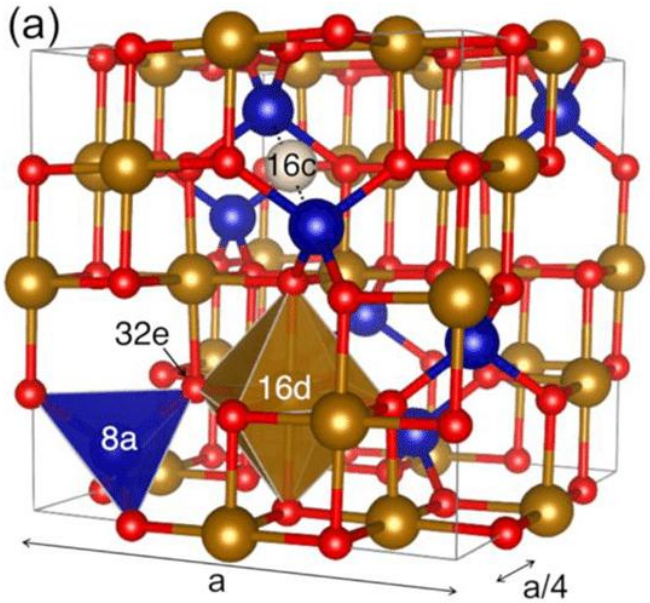

Figure 3. Cubic inverse spinel structures for magnetite, Fe_3O_4, iron in 16d shows octahedral sites (brown), Iron in 8a indicates tetrahedral sites (blue), and oxygen on 32e forming a cubic close-packed lattice (red) [5].

Nowadays, magnetite properties attract the researchers' interest, including those working on magnetic fluid catalysis, biotechnology, magnetic resonance imaging, and environmental remediation. Magnetic separations are effective methods to separate target magnetic particles from aqueous systems. The designs of the physical, chemical, and

surface properties of magnetic composite particles enable them for selective attachment of ions, molecules, macro-molecules, cells, or colloidal particles [46].

The magnetite (Fe_3O_4) NPs can be easily separated using a strong magnetic field. Because of its magnetic field property, a magnetite NPs is not only an adsorbent for toxic metal removal from solution, as shown in Figure 4, but also magnetically energized elements can be attracted and removed from the solutions. In addition, the toxic metals loaded on the isolated magnetic particles can be stripped off by, for example, acid eluent and the NPs can then be reused [47].

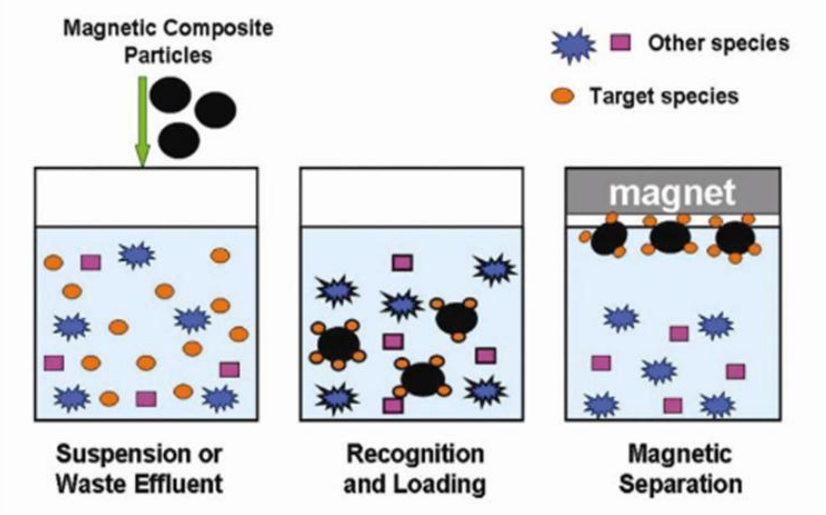

Figure 4. Illustration of magnetic separation technology in metal removal from aqueous media [47].

Applying MNPs for wastewater treatments have many advantages. Adsorption capacities of MNPs are relatively high due to its larger surface area. MNPs are rapid and straightforward separations of metal-loaded magnetic adsorbents from treated water by using an external magnetic field. Moreover, the secondary pollutants are not produced and the amount of chemicals used is reduced.

MNPs have been tested and found to be very effective in removing and recovering ions of heavy metals, such as Cu(II), Pb(II), Zn(II), Ni(II) and Hg(II) from water and industrials wastewater [48]. The addition of proper functional groups on MNPs enhanced potential applications in industrial wastewater. Many of the researchers have been used

MNPs for the removal of heavy metals from water and wastewaters. These have advantages due to their higher surface area to volume ratio, which leads to larger adsorption efficiency, fastest removal rates, and easy separations from solution by the magnetic field. The heavy metals could also subsequently be removed from the magnetic particles; therefore, they can be reused, and the metal also recovered [48].

Hu et al. (2005a) demonstrated without modification i.e., bare magnetite NPs (Fe_3O_4) for the removal of Cr(VI) from industrial wastewater. These NPs were synthesized through sol-gel methods, and the average diameter of the nanoparticles was about 10 nm [49]. Yean et al. (2005) and Mayo et al. (2007) used magnetic NPs as the adsorbents for the removal and recovery of both As(III) and As(V). The NPs in this case had been a small diameter, about 10 nm, and showed high efficiency for removal of As(III) and As(V) [50, 51]. Tuutijärvi et al. (2009) applied three types of magnetic nanoparticles (commercially available, sol-gel prepared, and monochemical made) for the removals of As(V) from water. The adsorption experiments were carried out with various particle sizes differing from 3 nm to 8 nm. However, these nanoparticles were not easily collected with the external magnetic field [52].

The characteristics of magnetic Nano-composite can be improved by silanization to form the particles with different functional groups, such as –SH, COOH, and NH_2. These functional groups were selected for effective, selective removal, and recovery of water pollutants. Furthermore, these functional groups target at the heavy metal ions, such as Cu, Pb, Zn, Ni, and Hg from aqueous solutions [48].

2.5.2.2 Modified MNPs for removal of heavy metals

Earlier studies by Matijevic′s group [53] confirmed that, oxalic and citric acid adsorbed to the hematite surface via chemisorption is highly pH dependent. In their studies, zeta potential measurements indicated that citric acid is bound either as a bi-dentate or a tri-dentate ligands.

Surface modification of MNPs using citric acid was reported by Sahoo et al. [11]. This work reported that, “citric acid showed adsorption to the surface of MNPs by coordinating through one or two functionalities of the carboxylate group”. The other uncoordinated carboxylic acid group on the surface of the coated NPs exposed to attach

to the solvent. The carboxylic acid group plays an important role in the hydrophilicity and surface charge of the material. Furthermore, the citric acid coated nanoparticles were observed to be in the super-magnetic regime and showed saturation. The super-magnetic character is influential for heavy metal removal and adsorbent separation from wastewater [12].

A studies by Sahoo et al., showed carboxylate groups of CA complexing with the iron (Fe) atoms on the magnetite surface that renders a partial single bond character to the C=O bond, weakening it, and shifting the stretching frequency to a lower value [53]. The citrate complex in $YFeO_3$ investigated by Todorovsk et al. is similar to this report [55]. It is observed that CA interacts to the magnetite surface by chemisorption of the carboxylate, citrate ions. In the other studies on aqueous Ferro fluid iron oxide nanoparticles synthesized by hydrothermal method, it is possible to reduce the particles size to about 8 nm by using citric acid as a reducing agent [55].

Singh et al. [57] prepared magnetite nanoparticles modified with succinic acid, ethylenediamine, and 2, 3-dimercaptosuccinic acid groups. The nanoparticles were applied for the removal of toxic metal (Cr (III), Pb (II), Co (II), Ni (II), Cu (II), Cd, and As(III)) and bacterial pathogens from water.

Liu et al. [57] synthesized humic acid surface coated magnetite nanoparticles (Fe_3O_4/HA) for the removal of heavy metal such as Hg (II), Pb (II), Cd (II), and Cu (II) from wastewater. Fe_3O_4/HA were prepared by the co-precipitation method. Adsorption of the heavy metals to Fe_3O_4/HA nanoparticle reached equilibrium with in short contact time and was found to be fitted in good agreement with the Langmuir adsorption model.

Wang et al. [58] synthesized amino-functionalized $Fe_3O_4@SiO_2$ MNPs with a core–shell structure to uptake heavy metal ions from an aqueous system. The amino-functionalized $Fe_3O_4@SiO_2$ nanoadsorbent exists with great adsorption capacity for aqueous Cu (II), Pb (II), and Cd (II) ions, resulting from the complexation of the metal ions by surface amino groups. The metal-loaded $Fe_3O_4@SiO_2–NH_2$ nanoparticles could be recovered readily from an aqueous solution by magnetic separation and regenerated easily by acid treatment.

2.6 Application of NPs for Pb metal adsorption

Various research activities in this area focused on the design and synthesis of NPs, their unique structures, and surface chemistry to achieve superior properties compared with conventional adsorbents.

Silica-based functionalized, nano-porous, and nanoadsorbent materials have high performance for environmental protection. A lot of good reviews have appeared in the literature dealing with the applicability of these superior adsorbents in wastewater treatment. For Pb(II) metal removal, the efforts had primarily been focused on the incorporations of the (-SH) groups to the mesostructure of silica nanomaterials [48]. Brown et al. (2000) found that one-step synthesis of thiol functionalized mesoporous structure with the pore diameters of around 2.5 nm. The highest Pb(II) metal sorption capacity was 206 mg/g. It was also found that the Pb(II) metal uptake rate was slower, and equilibrium condition was achieved within 24 hours [59, 60].

Mattigod (2007) produced novel materials by combining synthetic nanoporous substrate with a pore size of about 25 nm and high surface area approximated 1000 m^2/g with self-assembled monolayers of well-ordered thiol functional groups. As a result, the maximum removal capacities of lead metal were approximately 300 mg/g of sorbent with very fast kinetics (more than 95% of Pb was adsorbed in less than10 minutes of the contact time) [61]. Brown (1999) has explained the exciting point is that the mesoporous silica structure surface-modified with-SH organic groups are characterized by a very good selectivity for Pb(II) binding than corresponding amorphous sorbents [60].

Yoshitake et al. (2002) verified the removal efficiency of surface-functionalized monolayer ($Si{-}CH_2{-}CH_2{-}CH_2{-}SH$) for lead metal adsorption. Functionalized monolayers were highly efficient in removing Pb metal, pH has played a crucial role in the removal of Pb(II) by silica NPs. These experiments were usually performed between pH 4-6. Magnetic separation is an easy, effective method to separate targeted magnetic particles from complex multiphase systems. The magnetic NPs can also offer a high surface volume ratio, a simple method for the preparation and possibility for surface modifications. Even though, bare Fe_3O_4 NPs can be used effectively to remove toxic heavy metals, further surface modification with organic functional groups enhances their

adsorption performance [62]. The magnetite Fe_3O_4 NPs modified with humic acid were used to remove heavy metals, including Pb(II) metal. Sorption of the Pb(II) metal to Fe_3O_4/HA reached equilibrium in less than 15 minutes. More than 90% of Pb (II) was adsorbed using 50 mg/L of adsorbent at pH 6.0 [64]. Donia et al. (2008) tested the prepared magnetic chitosan resin modified with thiourea for Pb(II) metal adsorption, and their result shows that, about 90% of Pb^{2+} metals removal was achieved within 70 minutes and maximum uptake was 261.6 mg/g [63].

Due to their larger surface area, higher reactivity, and other described unique properties, magnetic and non-magnetic nanoparticles NPs have had a tremendous influence on the adsorption of Pb(II) metal. The following points need a further investigation:

- The optimal uptake conditions for engineering applications, such as pH value, the effect of adsorbent dosage, the initial metal ion concentration, and the effect of time, should be evaluated to enhance the performance of prepared NPs for treatment of real effluents with different chemical composition.
- Although, some previous studies have shown that, magnetite NPs modified with other surfactants has been well applied in Pb^{2+} ions removal and observed that excellent performance. However, CA is easy and efficient surface modifications for Pb^{2+} ions removal from wastewater were not well investigated.
- And most previous studies indicate disadvantages, such as NPs agglomeration, low adsorption capacity, slow kinetics, and inefficient reuse. All of these drawbacks will limit their practical application.

In this study, CA coated Fe_3O_4 nanoparticles (Cit-MNP) are developed for the removal of toxic Pb^{2+} ions from synthetic wastewater. Cit-MNPs are synthesized by a co-precipitation method with low cost and environmentally friendly iron salts. A novel low-cost magnetic sorbent material is prepared by coating Fe_3O_4 magnetic NPs with CA. The as synthesized Cit-MNPs were applied to remove heavy metal Pb^{2+} ions from wastewater. The physical and chemical characterizations of the synthesized coated Fe_3O_4 NPs were conducted. The reliability of MNPs in heavy metal removal was examined with the following characteristics: the sorption kinetics, the adsorbing capacity, material stability, effects of pH, nanoadsorbent dose, and metal ion concentration.

CHAPTER THREE

Materials and Methods

3.1. Materials

3.1.1 Chemicals

Ferric chloride or Iron (III) chloride monohydrate ($FeCl_3.H_2O$) (98.76%) (Supplied by Alpha Chemica, Mumbai, Maharashtra), ferrous chloride tetrahydrate ($FeCl_2.4H_2O$) (99%) (ATICO INDIA), lead nitrate ($Pb(NO_3)_2$) (99%) (Abron Chemicals, India), Citric acid ($C_6H_8O_7$) (99.5%) (Sigma Aldrich), ammonium hydroxide (NH_4OH) (28%), and hydrochloric acid (36%) (Supplied by LobaChemie Pvt. Ltd, India) were used. The solutions are prepared by using high purity De-ionized (DI) water with resistivity of 18.2 MΩ-cm as solvent. All the chemicals were analytical reagent grade.

3.2 Methods

3.2.1 Synthesis of magnetite nanoparticles

a. Preparation of bare magnetite nanoparticles

The bare Fe_3O_4 magnetic nanoparticles were synthesized using co-precipitation methods with little modification to A.K Bodbar et al. [66] and X.Liu et al. [68]. The synthesis procedure of nanoparticles is conducted in two separate 3-neck flasks. In the first one, 150 ml of distilled water was deoxygenated for 30 min by purging with nitrogen gas. In the second one, 50 ml of distilled water and 10 ml of 38% HCl were also deoxygenated with nitrogen gas. In the next step, to the first glass, 2.7 g of $FeCl_3 \cdot H_2O$ was added and bubbled with nitrogen gas, and to the second one, 1 g of $FeCl_2 \cdot 4H_2O$ was added. HCl was added to the iron (II and III) solutions to prevent the initial formations of the iron hydroxides. The solution was slowly added to the first flask from the second one (in the ratio of Fe^{2+}**:**Fe^{3+} = 1**:**2) and then stirred at 200 rpm at a temperature of 80 ˚c. Next, 20 mL of ammonium hydroxide (3M NH_4OH) was added drop-wise into the solution under vigorous stirring for 40 minutes until the pH value of the solution reached to the required pH (8, 10 or 11). To obtain nanoparticles in powder form, the black precipitated nanoparticles (Fe_3O_4) were separated by an external magnetic field and washed with

distilled water three times, then dried on a vacuum evaporator. A typical magnetite formation is described in (Equation 2) [66].

$$Fe^{2+} + 2Fe^{3+} + 8OH^{-} \rightarrow Fe(OH)_2 + 2Fe(OH)_3 \rightarrow Fe_3O_4\downarrow + 4H_2O \ldots\ldots\ldots\ldots\ldots\ldots (2)$$

b. Preparation of surface coated magnetite nanoparticles with citric acid

The bare magnetite (B-MNPs) nanoparticles prepared by the above procedures were well dispersed in 150 mL of methanol by ultra-sonication. After 15 minutes of sonication, a 0.01 M solution of citric acid surfactant was added to the mixture to modify the Fe_3O_4 MNPs [66]. The mixture was stirred at 300 rpm at 80 °C for 1 hour. The coated Fe_3O_4 MNPs were collected from the solution by magnetic field separation Figure 5. The as such prepared particles were washed with deionized water and dried on a vacuum evaporator [67]. The experiments were done repeatedly with the same procedure to get the required amount of nanoadsorbents. These particles are referred in this study as (Cit-MNPs)

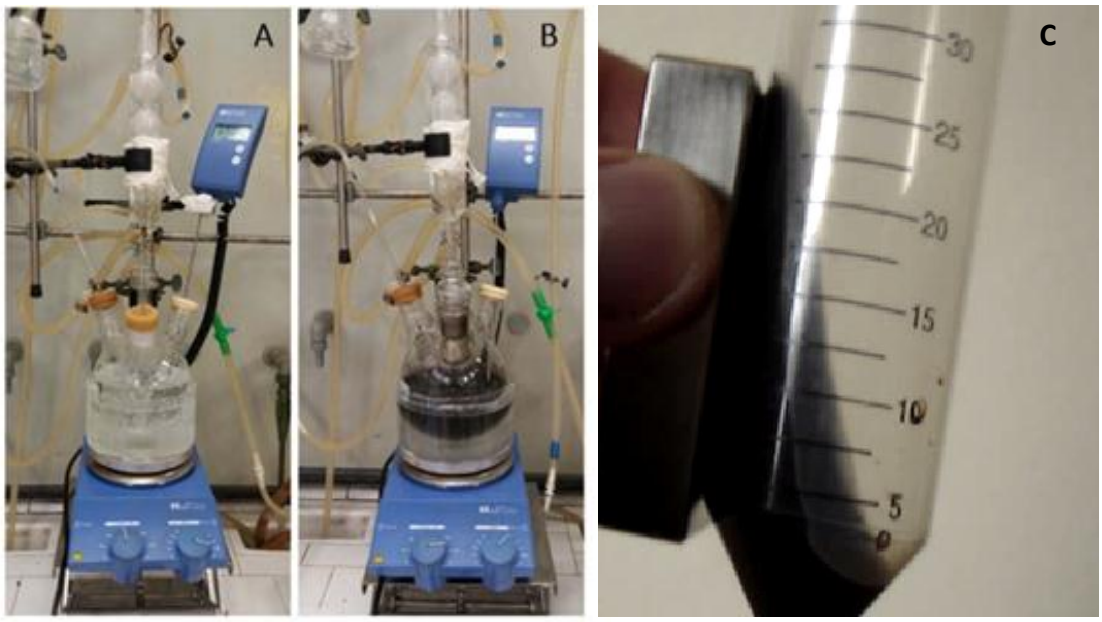

Figure 5. MNPs synthesis by co-precipitation technique, A: deoxygenating and heating, B: MNPs formation after precursor of ferric and ferrous solution addition, C: Black precipitated Fe_3O_4 powder collected by an external magnetic field

3.2.2 Characterization of the synthesized magnetite nanoparticles

The synthesized MNPs were characterized by using various techniques. The formation of Fe_3O_4 nanoparticles were examined using X-ray powder diffraction (XRD-700, Shimadzu, South Korea) at copper Kα radiation (λCu-Kα = 1.5418 Å), a scan speed of 3.0000 (deg/minute), voltage (40 kV), current (30 mA), and scanning range (4-80 °). The crystallite sizes of MNPs were calculated by applying Scherrer approximation equation:

$$D = \frac{K\lambda}{\beta \cos\theta}, \quad \ldots\ldots\ldots\ldots\ldots\ldots (3)$$

Where D is the crystallite size, K represents the shape parameter, which is 0.89 for magnetite NP, λ is standing for X-ray wavelength (0.15406 nm), β is full width at half maximum (FWHM) in radians in the 2θ scale, and θ is represented Bragg angle.

Fourier Transform Infrared (FTIR) Spectroscopy (Jasco-FTIR-6300), wavenumber range from 4000-400 cm^{-1} at 8 nm resolution was applied to identify functional groups on the adsorbent surface. The specific surface area, pore volume and average pore diameter size were obtained from N_2 adsorption-desorption isotherm by applying Brunauer-Emmett-Teller (BET) and Barett-Joyner-Halenda (BJH) techniques with micrometertics Tristar II 3020. ZetaSizer (Malvern P analytical Instrument Ltd, UK) performed at 25.0^{o}c, software version (V 8.02), serial number: MAL 1149420, for data collection and analysis in multiple narrow modes was used to determine surface charge potential and particle size distribution. Flame atomic absorption spectrometer (AAS) (model: ZEEnit 700P #150Z7P1025 Tech: Flame, with detection limit 0.06 ppm, energy = 71.5, PMT [V] = 298, slit width = 1.2 nm, lamp current = 3 mA) was used to determine the concentration of Pb^{2+} ions before and after adsorption experiments.

3.2.3 Adsorption experiments

a. Preparation of the stock solution

1000 mg/L Pb stock solution was prepared by dissolving 1.5990 g of lead nitrates in distilled water in a 1000 mL volumetric flask. A working solution of 50 mg/L was prepared by placing 50 mL of the stock solution in a 1000 mL volumetric flask and adding distilled water. Pb^{2+} ions standards were also prepared by pouring 10 mL of the stock solution in 100 mL volumetric flasks and adding distilled water. The standards of 1,

2, 3, and 4 mg/L were then prepared by placing 1, 2, 3, and 4 mL of the working solution in 100 mL volumetric flask and adding distilled water in measuring cylinder.

b. Batch mode adsorption experimental procedure

Batch adsorption experiments were applied using 250 mL Erlenmeyer flask with a 50 mL test solution at normal temperature following batch experimental procedure. The freshly prepared lead solution was placed in the flask covered tightly with aluminium foil (Figure 6). A weighed amount of adsorbents was then placed into the flasks. The flasks were then shaken in the orbital shaker at 200 rpm. The influence of various parameters such as adsorbent dose, pH, initial metal ion concentration, and contact time on the adsorption of Pb^{2+} ions were investigated in batch experiment approach. As these factors play a role in the adsorption process, optimizing each parameter is essential to estimate the maximum removal efficiency, equilibrium time, kinetics, and selection of an isotherm. The initial and final pH concentrations of Pb^{2+} ions were measured. All experiments were performed in triplicates, and the mean values are presented.

Percentage removal efficiency and adsorption capacity of MNPs nanoadsorbents were calculated using equation 4 and 5 as follows:

$$\text{Removal efficiency } \eta(\%) = \frac{C_o - C_e}{C_o} \, x \, 100, \quad \ldots\ldots\ldots\ldots\ldots\ldots \quad (4)$$

$$\text{Adsorption Capacity } (q_e) = \frac{(C_o - C_e)\, V}{m}, \quad \ldots\ldots\ldots\ldots\ldots\ldots\ldots\ldots \quad (5)$$

Where η is percentage removal efficiency, qe (mg/g) is the equilibrium adsorption capacity, Ce (mg/L) is the concentration of Pb^{2+} ion at equilibrium time, Co is the initial concentration of Pb^{2+} ion (mg/L), V is the volume of reaction solution, m is mass of the adsorbent,

Figure 6. a) Adsorbent samples with Pb^{2+} solution shaken in the rotary shaker. b) The remaining Pb^{2+} ions concentration for AAS analysis.

C. Optimization of pH on Pb^{2+} ions adsorption

pH values in the range 2 to 11 (2, 3, 4, 5, 6, 7 ,8, 9, 10 and 11) were tested for the adsorption of lead ions in a 50 mL solution of 50 mg/L lead (II) ions standard solution at 0.1 g/L of the nanoadsorbent. The pH was adjusted by the addition of 0.1 M HCl or 0.1 M NaOH regularly to avoid the formation of hydroxides by lead ions through precipitation (Figure 7). The adsorption experiment was carried out in a flask agitated using a shaker at 200 rpm for 120 minutes at normal temperature. And then, an external magnetic field was used to separate the magnetic NPs out of the lead solutions. The final concentration of Pb^{2+} ions was determined using AAS.

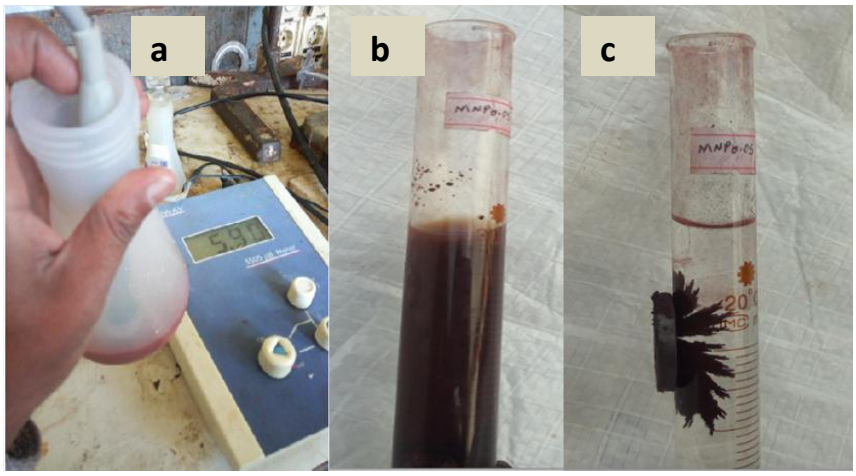

Figure 7. a) pH adjustment, b) nanoadsorbents in a solution before applied external magnetic field, c) separation of nanoadsorbents after applied external magnetic field.

d. Optimization of adsorbent dose

The effect of adsorbent dose on adsorption of metal ions was achieved by varying the adsorbent dose (0.05, 0.1, 0.15 and 0.2 g/L) for all adsorbate. 50 mg/L of 50 mL solution of the Pb^{2+} ions was used. The mixture was shaken at a constant shaking speed (200 rpm) for 120 minutes at ordinary temperature. The MNPs were isolated and separated by applying an external magnetic field at the end of the test, and the final concentrations of Pb^{2+} ions were analyzed by AAS.

e. Initial metal ion concentration optimization

The initial metal ion concentrations of lead (II) were carried out with varied from 25 to 200 mg/L, which is (25, 50, 100, 150, 200 mg/L). A constant of 0.1 g/L of the nanoadsorbent was added to 50 mL of the solution at a different concentration as mentioned above; the mixture was then shaken at a constant speed for 120 minutes at normal temperature, and the mixture was separated with an external magnetic field, and AAS was used to analyzed the final concentration of Pb^{2+} ions.

f. Contact time optimization

The influence of time on the interaction of the adsorbent with the lead ions was performed at optimum pH. 0.1 g/L of adsorbent was mixed with a 50 mL solution of lead ions an initial concentration of 50 mg/L. The mixture was then shaken constantly at time intervals of 20 minutes for 120 minutes (20, 40, 60, 80 and 120 minutes), and then the MNPs were separated with an external magnetic field. After separating the MNPs particles, the Pb^{2+} ions content in the supernatant was determined by AAS.

3.4.3 Fitting to Freundlich, Langmuir and Temkin isotherm models

Adsorption isotherm is mathematical model to describe the distribution of the adsorbate species on the adsorbent depending on a set of assumptions, either heterogeneity or homogeneity of nanoadsorbents [69]. Several isotherm models such as Langmuir, Freundlich, Temkin and D-R models have been used to evaluate experimental data for adsorption. However, the Langmuir, Freundlich and Temkin models are commonly applied by many researchers [70].

The Langmuir model assumes that there is no interaction among with the adsorbate molecules and the adsorption that is localized in a monolayer. The Freundlich isotherm model is an empirical relationship describing the adsorption of solutes from a liquid to a solid surface and assumes that there are different sites with several adsorption energies involved [69]. Temkin model is based on the assumptions that decrease in sorption energy would be linear with the coverage of surface by adsorbate molecule.

Generally, Langmuir, Freundlich and Temkin isotherm models are associated with the coverage or adsorptions of molecules on the solid surface to concentrations of a medium above the solid surface at a constant temperature. The experimental data of Pb^{2+} ions adsorption on MNPs at different pH values would be approximated by the isotherm models of Langmuir (3), Freundlich (4), and Temkin (5):

$$q_e = \frac{q_m b\, C_e}{1+b\, C_e} \text{ , ……..…..} \quad (6)$$

$$q_e = K_F C_e^{\,1/n} \text{ ,……} \quad (7)$$

$$q_e = \frac{R_T}{B_T} \ln K_T + \frac{R_T}{B_T} \ln C_e \text{ ,……..…..} \quad (8)$$

Where C_e is the equilibrium of lead ions concentration (mg/L), q_e is the capacity adsorbed (mg/g). q_m and b are Langmuir constants associated to adsorption capacity and energy of adsorption, determined from the y-intercept and slope of a plot ($1/q_e$ Vs $1/C_e$), respectively. K_F and n are the Freundlich constants that possess adsorption capacity and adsorption intensity calculated from the y-intercept and the slope of the linear graph plotted (log (q_e) Vs log (C_e)), respectively. K_T is the equilibrium binding constant (g/L), and B_T (J/mol) denote the Temkin constant that is related to heat of adsorption, the isotherm constant K_T calculated by plotting the linear plot of q_e Vs ln C_e.

The linear form of the Langmuir and Freundlich Equations (6) and (7) can be written as

$$\frac{1}{q_e} = \frac{1}{(q_m b)\, C_e} + \frac{1}{q_m} \text{ , ……} \quad (9)$$

$$\log q_e = \left(\frac{1}{n}\right) \log C_e + \log K_F \text{ , ……...} \quad (10)$$

3.4.4 Isotherms model for Pb^{2+} ions adsorption

The initial concentrations of the Pb^{2+} ions ranged between 25 and 200 mg/L. A 0.1 g/L of the Fe_3O_4 nanoadsorbents were shaken with Pb^{2+} ions standards at the value of pH 5 for 60 minutes (optimized contact time) at 25 °C on a rotatory shaker to ensure removal equilibrium was reached. The removal of the adsorbent was done, followed by the determination of Pb^{2+} ions concentrations by AAS.

3.4.5 Modeling of kinetics adsorption

The modeling of kinetic data is fundamental for the relevant of industrial application of adsorption since it gives information for comparison among different nanoadsorbent materials under different operational conditions for designing and optimizing operational conditions for pollutants to remove from wastewater systems [70].

The study of sorption kinetics model is applied to describe the adsorbate uptake rate, and this rate clearly controls the residence time of adsorbate at the solid-liquid interface. In order to evaluate the mechanism of sorption of Pb^{2+} by the MNPs, the pseudo- first-order equation, and the pseudo-second-order rate equation are calculated by the following equations, respectively:

$$\mathrm{Log}(q_e - q_t) = \mathrm{Log}(q_e) - \frac{K_1 t}{2.303}, \quad \text{..... (11)}$$

$$\frac{t}{q_t} = \frac{1}{K_2 q_e^2} + \frac{t}{q_e}, \quad \text{..... (12)}$$

Where q_t is the adsorption capacity at the time (mg/g), K_1 the Lagergren rate constant of the adsorption (1/minute), k_2 is the rate constant of the pseudo-second-order sorption ($g \cdot mg^{-1} \cdot minute^{-1}$). If the kinetic models are applicable to the experimental data, then q_e is calculated from y-intercepts, and K_1 and k_2 can be calculated from the slopes of the linear plots log ($q_e - q_t$) versus t, and t/q_t versus t of the above equations, respectively.

The adsorption studies were carried out by adding 0.1 g/L of B-MNPs and Cit-MNPs nanoadsorbents into 50 ml conical flasks containing 50 mg/L Pb^{2+} ions solutions. The mixtures were shaken for different contact times from 20 to 120 minutes. The Pb^{2+} ions concentrations in the supernatants were determined after 20, 40, 60, 80 and 120 minutes of agitation by air acetylene flame atomic absorption spectrophotometer (AAS).

CHAPTER FOUR

4. Results and Discussion

4.1. Characterization of magnetite nanoparticles

4.1.1 XRD pattern analysis of Fe_3O_4 NPs

The synthesized B-MNPs and Cit-MNPs were analyzed using XRD (Figure 8). XRD spectra of the synthesized MNPs (Fe_3O_4) were examined to determine the magnitude of crystallinity. The formation of inverse spinel cubic Fe_3O_4 nanoadsorbents was confirmed from the major diffraction peaks obtained at 2θ = 18.24, 30.56, 35.86, 43.46, 54.01, 57.38, 63.01, and 74.46 and those correspond to the crystallographic planes of (111), (220), (311), (400), (422), (511), (440), and (533). The spectra obtained were fairly near to the Joint Committee on the Powder Diffraction Standards (JCPDS File No. 65-3107) without any noticeable impurity. The presence and appearance of sharp and intense peaks confirmed the formation of highly crystalline MNPs nanoparticles.

The crystallite size was calculated from the full width at half maximum (FWHM) of the highest reflection at (311) peak. Applying the Scherrer approximation, this assumes the small crystallite size that can be the cause of line broadening [71]. By taking the strongest intensity peak, namely the (311) plane, at 2θ = 35.86 (0.601 radians), for which FWHM is 0.2098 (0.0076 radians), the prepared sample crystal size was calculated, about 62.3 nm.

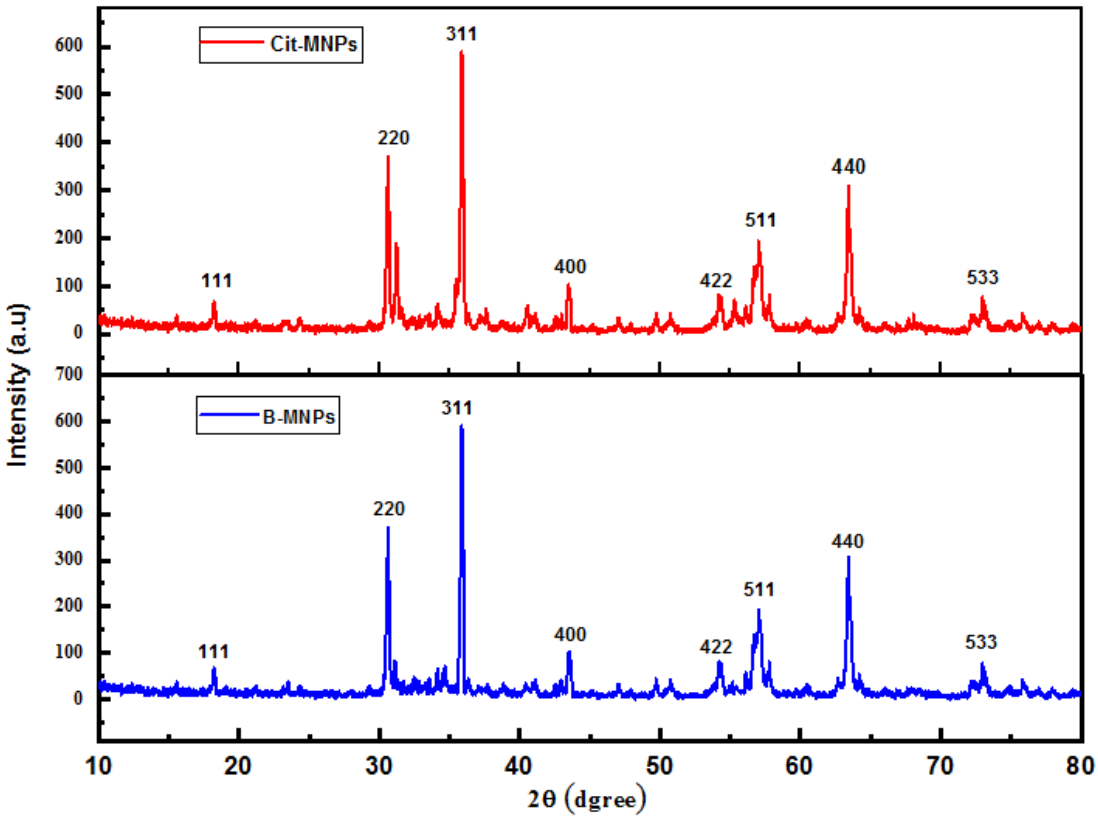

Figure 8. XRD spectra of synthesized MNPs, showing formation and crystal structure of Fe_3O_4.

4.1.2 Brunauer–Emmett–Teller (BET) analysis of MNPs

The specific surface area, pore size and volume distribution were studied by BET and BJH methods in nitrogen adsorption-desorption environment. The particulate properties of the samples, such as surface area, pore size and volume distributions are listed in table 3. Adsorption-desorption isotherms of the two samples correspond to type IV isotherm as shown in Figure 9. The BET surface areas were 73.35 m^2/g and 113.86 m^2/g, respectively for B-MNPs and Cit-MNPs. BET calculation applied to the determination of the pore volume and average pore diameter which were 0.41 cm^3/g and 26.31 nm for B-MNPs and 0.23 cm^3/g and 19.52 nm for Cit-MNPs, respectively. The smaller surface area of B-MNPs could be due to the aggregation of NPs. The higher surface area and varying pore size of Cit-MNPs is due to deposition of CA coat on the surface of MNPs and makes it beneficial for the Cit-BMNPs as they help in large Pb^{2+} ions loading and help improving removal efficiency to heavy metals from wastewater. It is true that, a large surface area

will improve the adsorbing capacity and removal efficiency because of the availability of more active sites on the surface of the MNPs [48].

Table 3. BET and BJH surface area, pore sizes, and pore volume distribution of the as synthesized MNPs sample.

Sample	BET (m^2/g)	Pore size (nm)	Pore volume (cm^3/g)
B-MNPs	73.35	26.31	0.41
Cit-MNPs	113.86	19.52	0.23

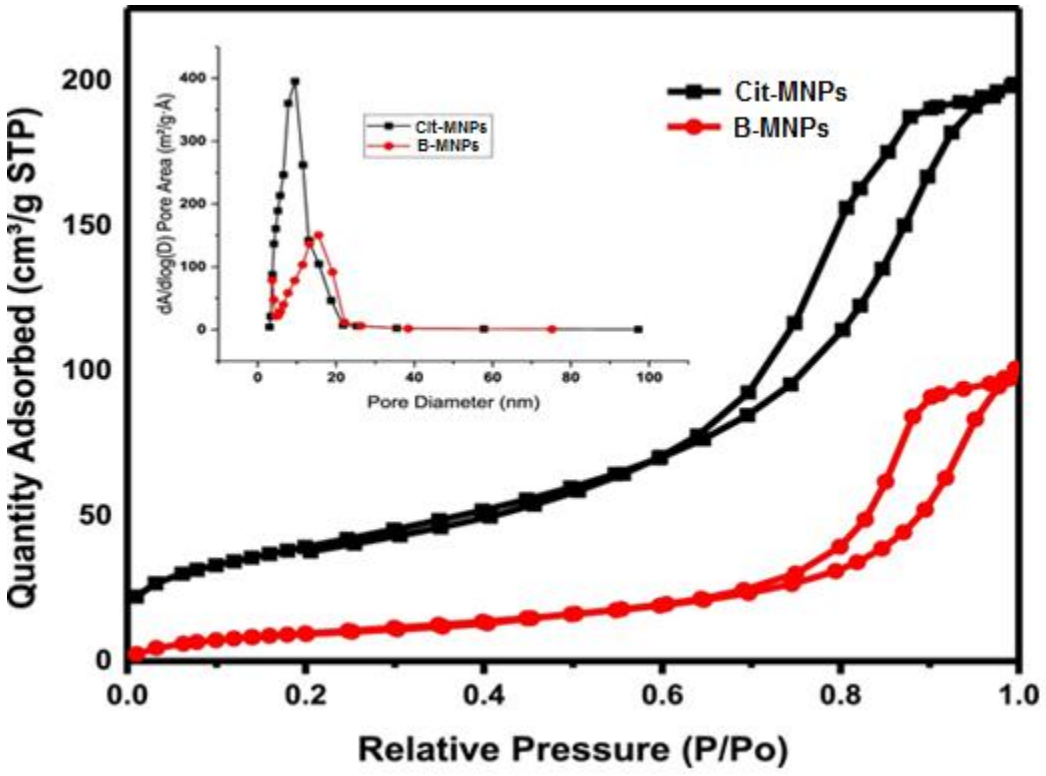

Figure 9 . Nitrogen adsorption and desorption isotherms of B-MNPs and Cit-MNPs.

4.1.3 Zetasizer analysis of MNPs

Zeta potential (ζ) is a meaningful technique for understanding nanoparticles′ surface and their ability to be stable in a solution. Dispersion stability can be characterized by the zeta potential value in (mV) [72]. Zeta potential value values from 0 to ± 5 mV can be a reason for rapid agglomeration and NP suspension precipitation. The zeta potential values ranging from ±10 to ±30 mV are accountable for the threshold beginning to instability, which means that nanoparticle has started agglomerating due to interparticle interactions,

and it might result in physical instability. Usually, for zeta potential values greater than +30 mV or less than negative -30 mV, particles have high stability, and ± 40 to ± 60 mV shows the excellent stability of NPs suspension related to a high charge on their surface [73].

The zeta potential of synthesized magnetite nanoparticles (Fe_3O_4) modified with citric acid was found to be negative -36.5 mV (Figure 10). Hence, the synthesized magnetite nanoparticles denote high stability of colloidal Fe_3O_4 (Cit-MNPs). In addition, the negative charges of the Zeta potentials were because of the electrostatic stabilization delivered by strong adsorption (binding) of the citrate ions on MNPs surface.

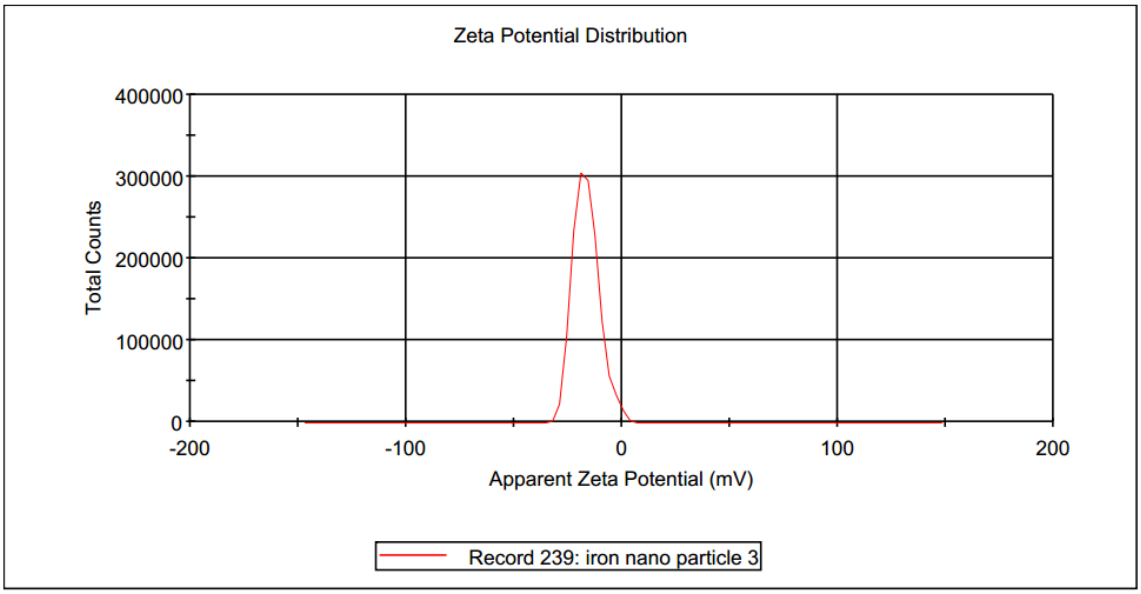

Figure 10. Zetasizer potential distributions of Cit-MNPs

Similarly, the zeta potential of the synthesized B-MNPs (Fe_3O_4**)** were measured and found to be positive +11.4 mV (Figure 11). Hence, the result suggests that the unmodified magnetite nanoparticles were aggregated and instable in a solution. There was a close agreement among the obtained results of this study and the results previously reported by Wei et al. [78].

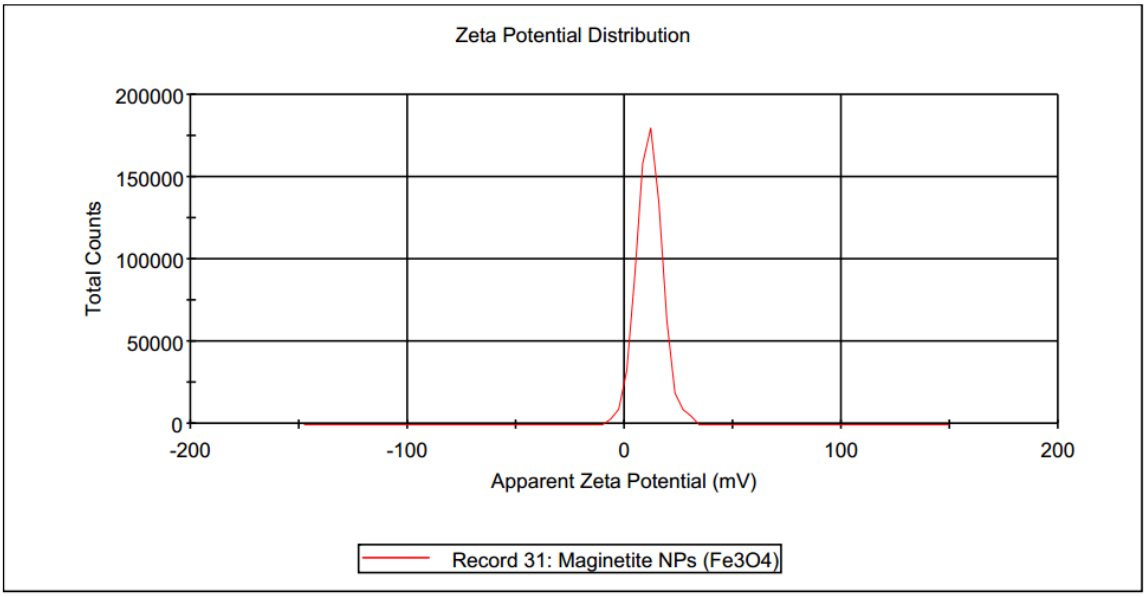

Figure 11. zitasizer potential distributions of B-MNPs

The average particles diameter of citric acid coating (Cit-MNPs) (±SD) was 82.14 ± 0.52 nm (Figure 12). Only one peak in the plot (Fig. 12) means the synthesized MNPs are highly mono-dispersed in an aqueous solution the reason for this is, probably due to the expected effect of the CA coating preventing from nanoparticles aggregation.

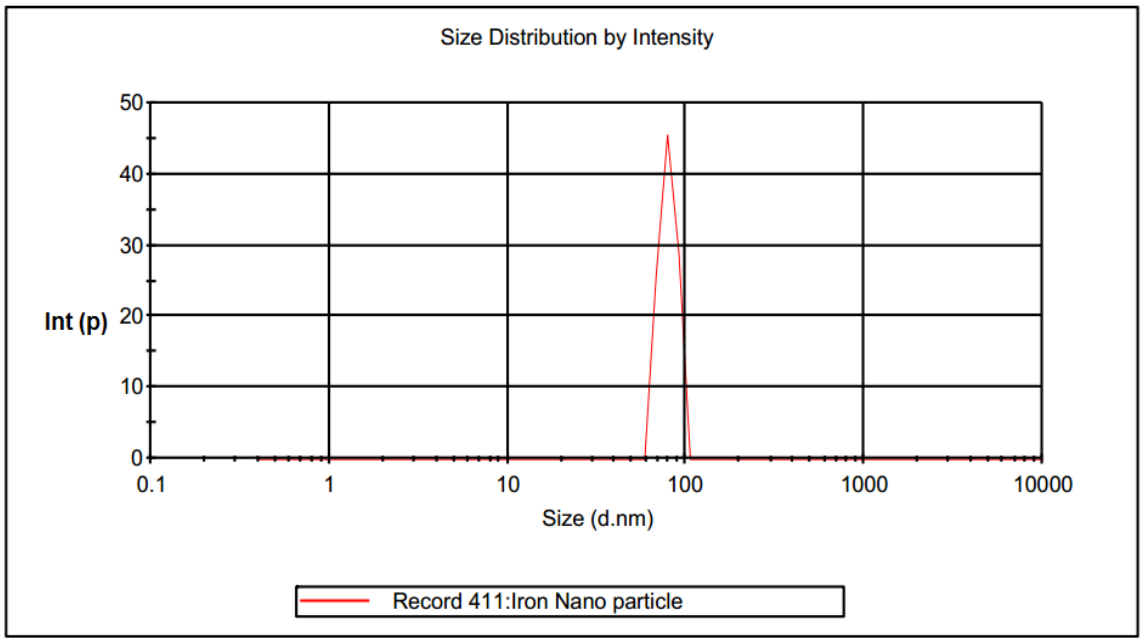

Figure 12. Zetasizer particle size distribution of Cit-MN

4.1.4 FT-IR analysis of Fe_3O_4 NPs

FT-IR was used to analyze the functional groups on the surface of the magnetite nanoparticles MNPs before and after modification with citric acid [74].

The IR spectra for pure CA are well resolved (Figure 13). However, those of the Cit-MNP are rather broad and few. The 1710 cm^{-1} peak assigned to the C=O vibration (asymmetric stretching) from the COOH group of CA shifts to an intense band at about 1650 cm^{-1} for Cit-MNP. This indicates that the binding of CA radicals on the surface of MNPs (Fe_3O_4) by chemisorptions of carboxylate (citrate) ions. Iron (F_e) atoms on the surface of MNPs form complexes with carboxylate groups of CA and be translating the partial single bond character of the C=O bond. This causes in weakens the C=O bond, which shifts the stretching frequency to a lower value [75]. A large and intense peak at 3498 $cm^{-1}$was assigned to the structural OH groups of citric acid and the traces of molecular water. Furthermore, the vibrational modes appearing at 1070, 1270, and 1440 cm^{-1} in Cit-MNP correspond to the symmetric stretching of OH, symmetric stretching of C–O, and COO^- group of CA, respectively [54]. The strong IR band observed at around 528 cm^{-1} in Cit-MNP can be described as the Fe–O stretching vibrational mode of the tetrahedral positions to spinel inverse structure of the magnetite nanoparticles (Fe_3O_4) [54, 56].

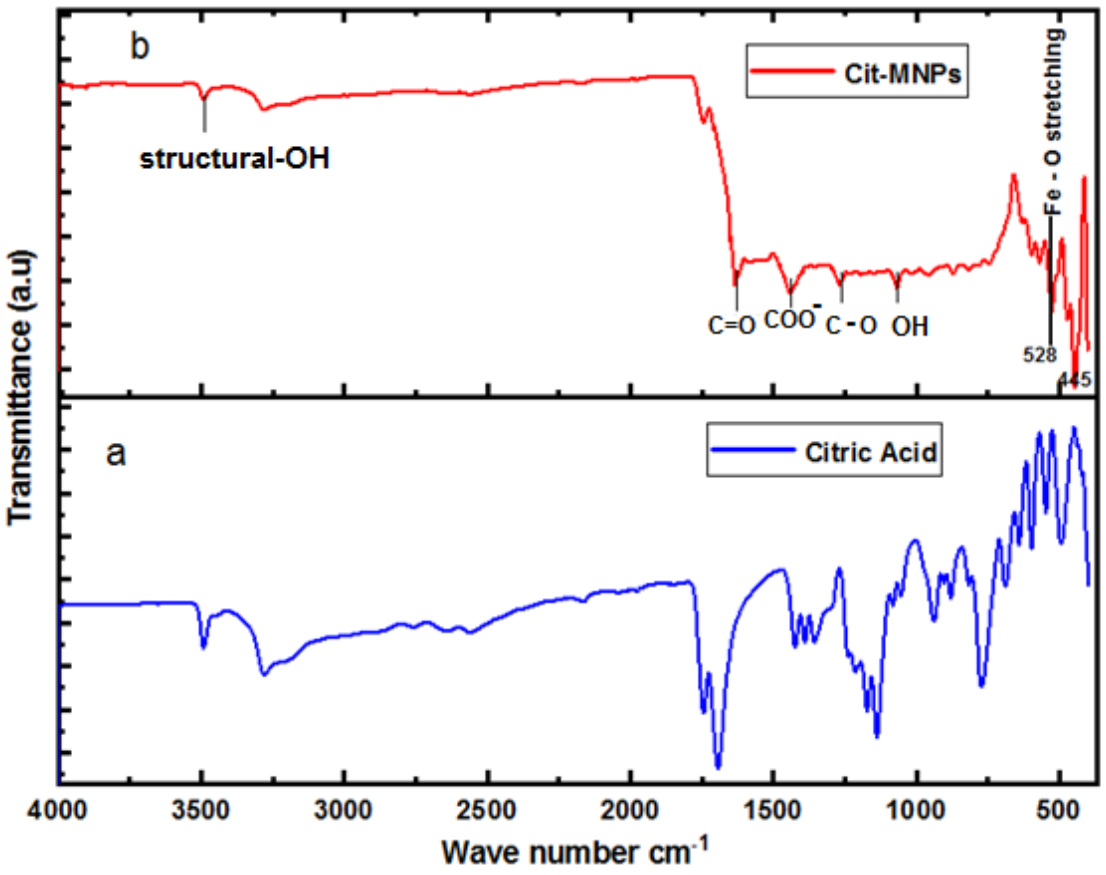

Figure 13. FTIR spectra of pure citric acid (CA) and modified Cit-MNP.

4.3 Optimization of parameters for adsorption of Pb^{2+} ions

The adsorption of Pb^{2+} ions from synthetic wastewater using synthesized MNPs was studied by batch experiments approach. The optimal conditions for the maximum removal efficiency of Pb^{2+} ions were investigated.

4.3.1 Effects of pH on Pb^{2+} ions removal

The pH of a solution has a valuable influence on Pb^{2+} ions uptake as it affects the surface charge of the sorbent, the degree of ionization, and the speciation of the lead ions. Hence it is important to understand whether the surface of the adsorbent is positively charged or negatively charged, depending on different pH values [76].

The conditions at which effect of pH was studied on the adsorption of the metal ion by contacting adsorbent dose, 0.1 g/L; initial metal ion concentration, 50 mg/L; contact time, 60 minutes; and at room temperature

From (Figures 14 and 15) and Appendix A.1, the adsorption of lead ions was very low at pH 2 for B-MNPs and Cit-MNPs. This is due to the competition for binding sites between Pb^{2+} and H^{+} ions. The Pb^{2+} adsorption efficiency increased linearly from pH 2 to 5, then stabilized between pH 5 and 7 for both MNPs. Beyond pH 7, the adsorption rate rises may be due to some precipitation of Pb $(OH)_2$. Higher values of pH > 7 were avoided due to hydrolysis and precipitation of Pb^{2+} ions. Therefore, all the series experiments were limited to a maximum of pH 7.

The maximum Pb^{2+} ions removal efficiency for Cit-MNPs was 96.3% and 83.5% for B-MNPs at pH 5. The low adsorption of Pb^{2+} ions at pH 2 were because of the high concentration and high mobility of H^{+} ions in the solution, which competed with Pb^{+2} ions for the adsorption sites; this caused to obstruct the adsorption of Pb^{+2} ions. The protonated of adsorbent sites were incapable of binding the Pb^{+2} ions due to the lack of electrostatic attraction between positively charged sites.

The functional groups essentially hydroxyl (-OH) and carboxyl (-COOH) on the surface of MNPs at lower pH get protonated by H^{+} ions leading to the net positive charges on the surface of the adsorbent as described by the equation:-

$$ROH + H^{+} \rightarrow ROH_2^{+} \quad \text{(13)}$$

$$RCOOH + H^{+} \rightarrow RCOOH_2^{+} \quad \text{(14)}$$

Consequently, this was established the repulsive force between Pb^{+2} ions cationic species and the positively charged surface of nanosorbent, which hinders the sorption process. Whereas, at a relatively higher pH value, the removal efficiencies of the adsorbent were greatly facilitated due to the deprotonation of (-OH) and (-COOH) groups on MNPs surfaces, leading to a negative charge on the surface, as shown by the following equation. In contrast, the predominant Pb^{2+} ions are positive; therefore, the adsorption increases.

$$RCOOH + OH^{-} \rightarrow RCOO^{-} + H_2O \quad \text{(15)}$$

$$ROH + OH^{-} \rightarrow RO^{-} + H_2O \quad \text{(16)}$$

Hence, it can be concluded that the adsorption of lead onto the selected adsorbents is dependent on pH values.

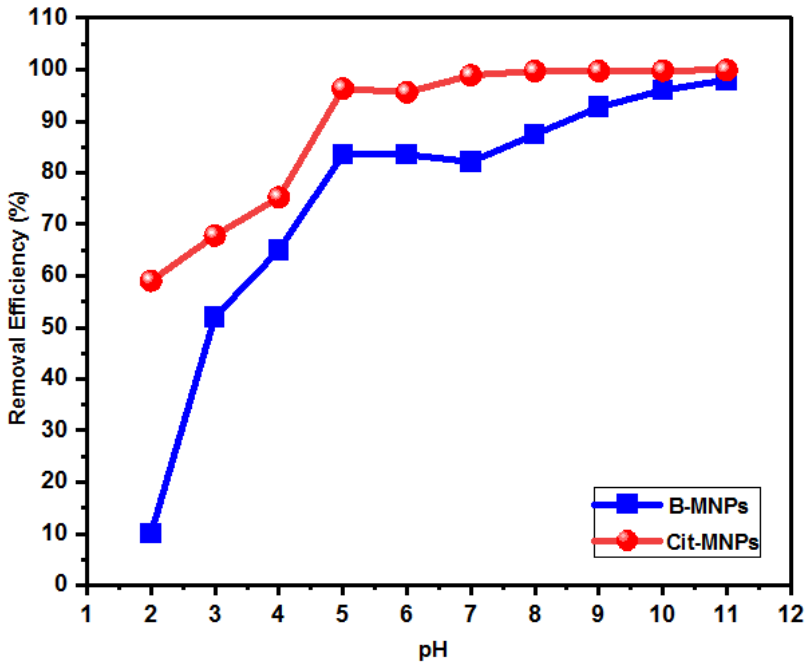

Figure 14. Effects of pH on Pb^{+2} removal efficiency onto B-MNPs and Cit-MNPs [initial Pb^{+2} concentration, 50 mg/L; adsorbent dose, 0.1 g/L; contact time, 60 minutes; and at room temperature]

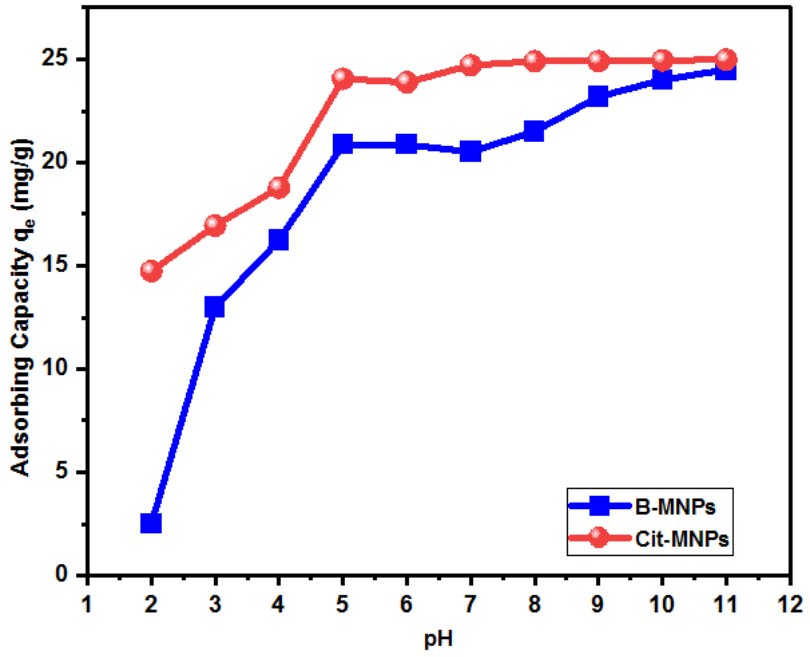

Figure 15. Effects of pH on Pb^{+2} adsorption capacity onto B-MNPs and Cit-MNPs [initial Pb^{+2} concentration, 50 mg/L; adsorbent dose, 0.1 g/L; contact time, 60 minutes; at room temperature]

4.3.2 Effect of MNPs adsorbent dosage

The experiments were conducted to assess the affinity of MNPs at different dosages toward Pb^{2+} ions. The initial adsorbent dosages of MNPs (B-Fe_3O_4) and (Cit-Fe_3O_4) was adjusted to be within the range of 0.01 to 0.2 g/L in 50 g/L Pb^{2+} ions solution. The amount of Pb^{2+} ions adsorbed is achieved greater using Cit-MNPs when compared to B-MNPs (Figure 16 and 17) and appendix A.2.

B-MNPs recorded lower percentage removal compared to Cit-MNPs, about 83.5% and 83% at 0.05 g/L and 0.1 g/L adsorbent dosage, respectively. Further increase in mass of B-MNPs adsorbent dose, the adsorption efficiency and capacity got decreased due to the reason that only a fraction of active sites is available for higher doses because of aggregation of nanoparticles, which reduced in total surface area of nanoadsorbents and thus decreased Pb^{2+} ions sorption. Similar results were reported by R. Singh et al. [75].

Cit-MNPs recorded the highest percentage removal of Pb^{2+} ions, about 96.7 % at a dosage of 0.1 g/L. On increasing the initial Cit-MNPs dosage, the percentage removal also increased up to the optimum value is reached. Due to the fact that, more reaction and binding sites are available for Pb^{2+} ions to be adsorbed. CA used as a stabilizer during the preparation of the Fe_3O_4 particles is able to efficiently reduce particle aggregation, having effective particle size, resulting in much greater specific surface area and adsorption sites [76]. Beyond the optimum value of nanoadsorbents the percentage removal remains constant due to the saturation of adsorption sites reported by [77].

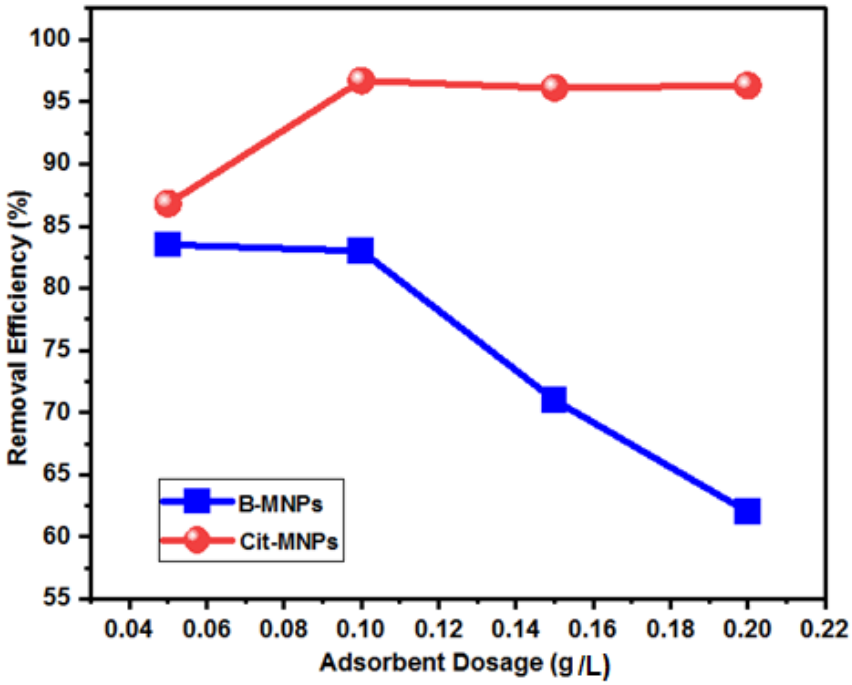

Figure 16. Effects of adsorbent dose on Pb^{+2} removal efficiency onto B-MNPs and Cit-MNPs [initial Pb^{+2} concentration, 50 mg/L; pH 5; contact time, 60 minutes; and at room temperature]

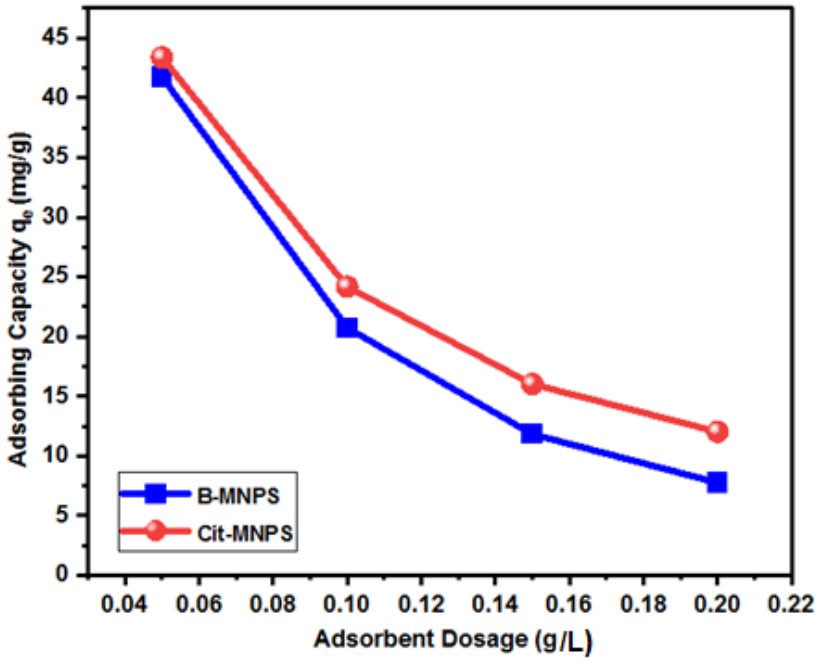

Figure 17. Effects of adsorbent dose on Pb^{+2} adsorption capacity onto B-MNPs and Cit-MNPs [initial Pb^{+2} concentration, 50 mg/L; pH 5; contact time, 60 minutes; and at room temperature]

4.3.3 Effects of initial concentration of Pb^{2+} ions

The percentage removal of Pb^{2+} ions adsorbed by B-MNPs and Cit-MNPs was influenced by the initial concentrations of Pb^{2+} ions in aqueous solutions. The initial concentrations of Pb^{2+} varied from 25 to 200 mg/L while maintaining the adsorbent dosage at 0.1 g/L. (Figures 18 and 19) and Appendix A.3 show the effect of initial concentration on percentage removal of Pb^{2+} ions.

Nanoadsorbent up taking capacity depends on the starting metal ions concentration. At higher adsorbate concentrations, more Pb^{2+} ions molecules are accessible to react with the surface of MNPs. The results showed that the sorption of adsorbate was quick at the preliminary stages (relatively rapid initial rate of adsorption). The significant percentage removal of Pb^{2+} ions was achieved, up to 84.5% and 96.5% at the same initial metal ion concentration of 50 mg/L for B-MNPs and Cit-MNPs, respectively.

It was observed that the surface of Fe_3O_4 modified with CA is an efficient adsorbent for the removal of toxic metal Pb^{2+} ions than unmodified magnetic nanoparticles. The result indicates that beyond the concentration of 50 mg/L, the sequestration rate of Pb^{2+} ions was considerably followed by a slow approach to equilibrium. This may be accredited to the inaccessibility of empty sites and saturation of functional group sites on the surface of the adsorbent [75]. These results agree with the already reported works [76].

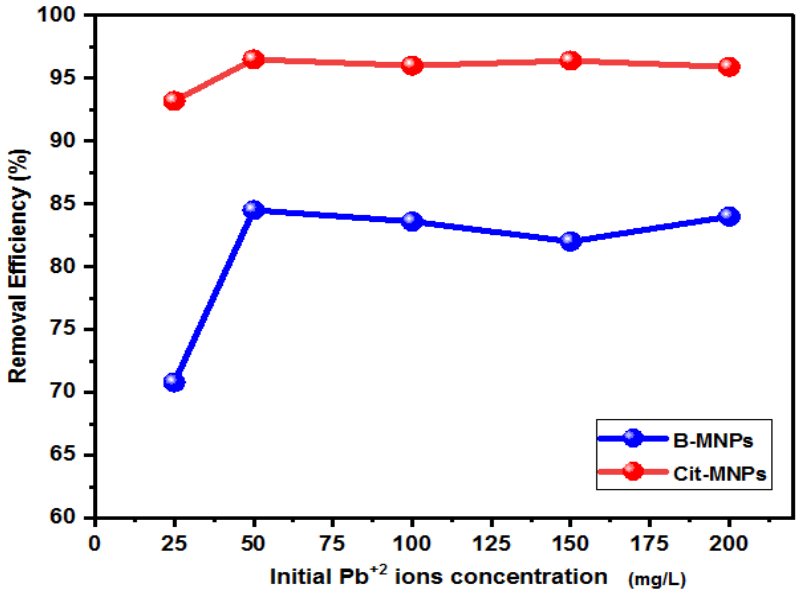

Figure 18. Effects of initial metal concentration of Pb^{+2} removal efficiency onto MNPs [pH 5; adsorbent dose, 0.1 g/L; contact time, 60 minutes; and at room temperature]

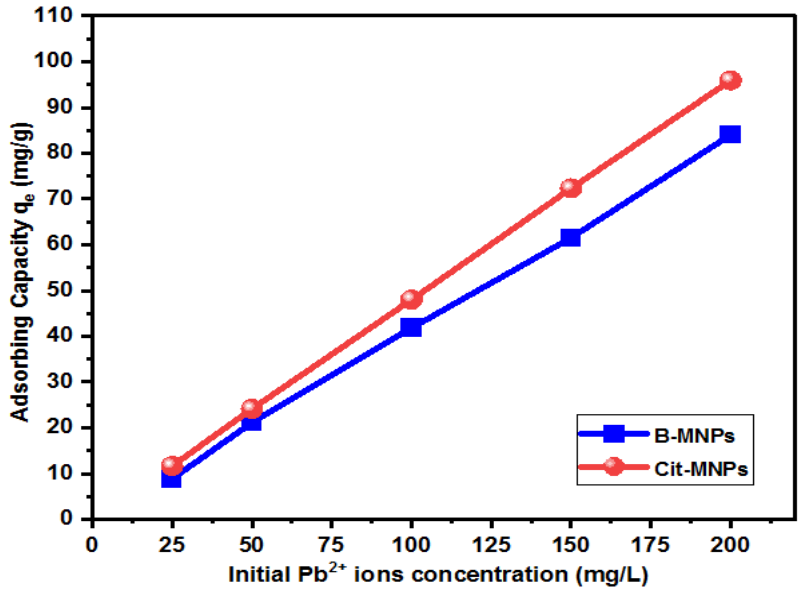

Figure 19. Effects of initial concentration of Pb^{+2} ions of adsorption capacity onto B-MNPs and Cit- MNPs [pH 5; adsorbent dose, 0.1 g/L; contact time, 60 minutes]

4.3.4 Effects of contact time

Maintaining the magnetite nanoadsorbent dosage, pH, and metal ion concentration at constant values, the effect of varying the adsorption time was investigated. The result indicated that the lead adsorption increases with contact time. As shown in Figures (20 and 21) and Appendix A.4 during the first 60 minutes, the amount of Pb^{2+}adsorbed onto both bare nanoadsorbent (B-MNPs), and modified magnetite nanoadsorbent (Cit-MNPs) increased rapidly. Subsequently, after 60 minutes the Pb^{2+} ions adsorption rate rises gradually and stabilized. The percentage removal efficiency was 96.1% and 83.6% by using Cit-MNPs and B-MNPs, respectively at adsorption time of 60 minutes. After 60 minutes, the Cit-MNPs an adsorption capacity of Pb^{2+} ions was slightly increased. Therefore, a contact time of 60 minutes was taken as the optimum adsorption time.

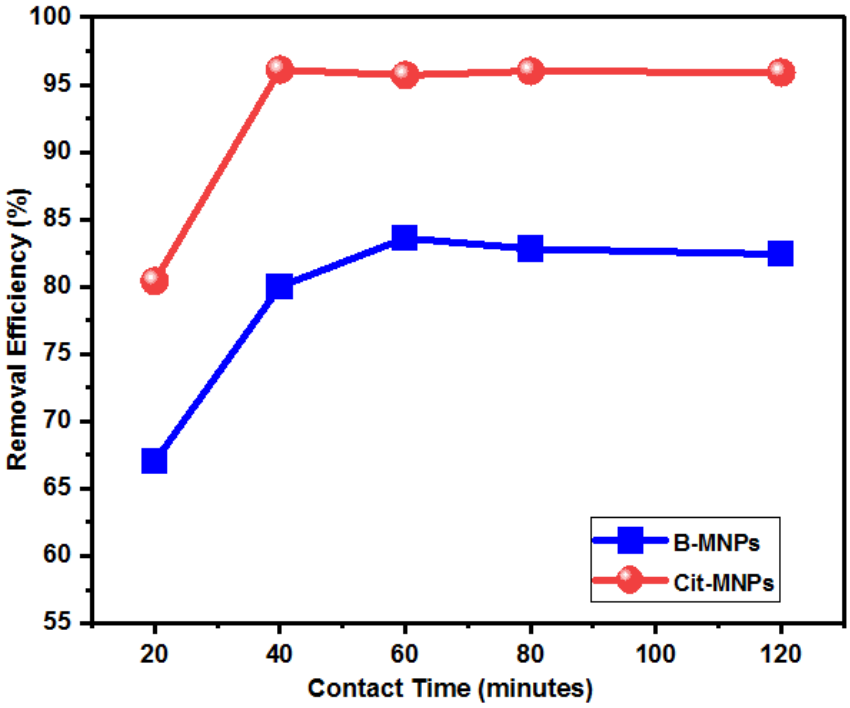

Figure 20. Effects of contact time on Pb^{+2} removal efficiency onto B-MNPs and Cit-MNPs [initial Pb^{2+} concentration, 50 mg/L; pH 5; adsorbent dose, 0.1 g/L]

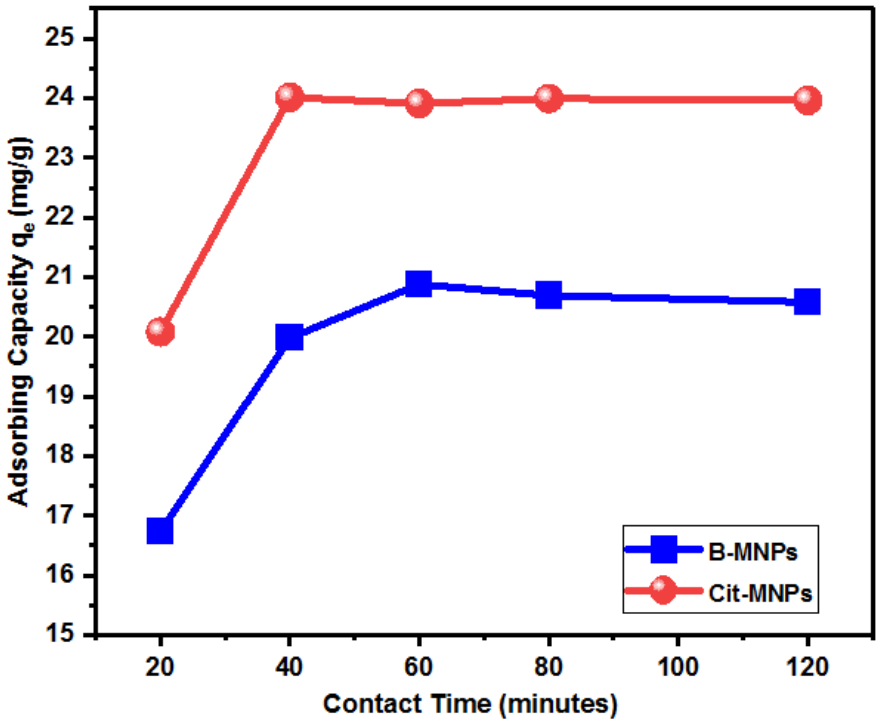

Figure 21. Effects of contact time on Pb^{+2} adsorption capacity onto B-MNPs and Cit-MNPs [initial Pb^{2+} concentration, 50 mg/L; pH 5; adsorbent dose, 0.1 g/L]

4.4 Exploration of the appropriate isotherm model

The adsorption isotherm describes the equilibrium distribution of adsorbate onto the adsorbent at a constant temperature. Adsorption isotherms are useful to state surface properties and adsorption mechanisms. To derive data for the determination of the adsorption isotherm, the following parameters were employed: Initial concentrations of Pb^{2+} ions (25, 50, 100, 150, and 200 mg/L) were used for Cit-MNPs and B-MNPs nanoadsorbents at a dosage of 0.1 g/L, at pH 5, and at the optimized time (60 minutes), respectively (Table 5).

The results obtained for Pb^{2+} ions adsorptions using the two adsorbents were fitted in Langmuir, Freundlich and Temkin isotherm model. The constants obtained are summarized in (Table 4), and the equilibrium concentration (C_e) is shown in Appendix B.

For B-MNPs, the Langmuir and Freundlich models showed good agreement to the experimental data with the correlation coefficient, R^2, values recorded at 0.94 and 0.98, respectively (Figures 22 and 23). The maximum adsorption capacities, q_{max}, of Pb^{2+} ions were found to be 111.1 mg/g. Therefore, this points out the applicability of monolayer and multilayer coverage of Pb^{2+} ions on the surfaces of the B-MNPs nanoadsorbents. Hence, there is an effective interaction between synthesized B-MNPs and Pb^{2+} ions.

Similarly, (Figures 22 and 23) presented the Langmuir and Freundlich linear fit for Cit-MNPs. The values of correlation coefficient $R^2 = 0.94$ were recorded for Langmuir, and $R^2 = 0.98$ for the Freundlich model. The maximum adsorption capacity (q_{max}) was 200.0 mg/g. The good correlation coefficient of both isotherm models also indicates that Pb^{2+} ions adsorbed to the surface of Cit-MNPs. However, in the comparison, adsorption of Pb^{2+} ions on adsorbents fits the Freundlich model better than the Langmuir model. By considering the adsorption coefficient of b, this is related to that apparent energy of adsorption for Pb^{2+} ions on Cit-MNP (0.06 L/mg) were greater than on B-MNPs (0.021 L/mg). Therefore, the energy of adsorptions is more favorable on Cit-MNPs than B-MNPs. Hence, Cit-MNPs had the highest adsorption capacity due to surface modification, increasing the binding sites of the adsorbent. Furthermore, the dimensionless Freundlich constant of n >1 indicates that adsorption was favourable on the heterogeneous surfaces. The 1/n is a function of the strength of the adsorbent to the

adsorption process. If the value of n = 1, then the partition among the two phases are independent of the concentration. If the value of 1/n is below one, it indicates normal adsorption takes place. On the other hand, the value of 1/n being above one indicates cooperative adsorption [76]; the smaller 1/n, the greater the expected heterogeneity. The adsorption intensity (1/n) = 0.9 showed that the adsorption of Pb^{2+} ions on the surface of Cit-MNPs was favourable. Therefore, it is verified that MNPs have a greater potential to be a good adsorbent for removing Pb^{2+} ions in wastewater treatment.

Moreover, Figure 24. Shows that the Temkin isotherm model for Pb^{2+} ions adsorptions onto B-MNPs and Cit-MNps. The adsorption result obtained for Pb^{2+} ions on B-MNPs and Cit-MNPs fitted with correlation coefficient (R^2) value of 0.92 and 0.95, respectively. Temkin adsorption equilibrium binding energy constant, $K_{T,}$ for B-MNPs and Cit-MNPs, is 0.2 L/mg and 0.9 L/mg, respectively. This suggests that the modified Cit-MNPs have higher adsorbent potential for Pb^{2+} ions in wastewater. The smaller K_T value for B-MNPs indicated that there is an indirect interaction between adsorbate metal ions and adsorbent particles which related to the linear decrease in the heat adsorption of all molecules on the surface.

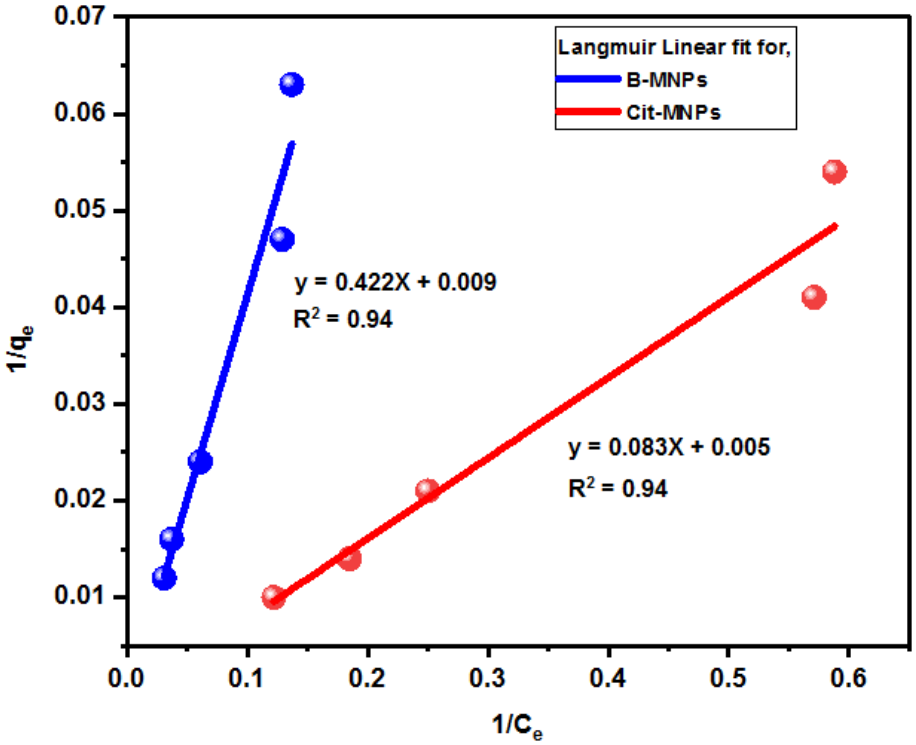

Figure 22. Fitting to Langmuir adsorption isotherm for B-MNPs and Cit-MNPs

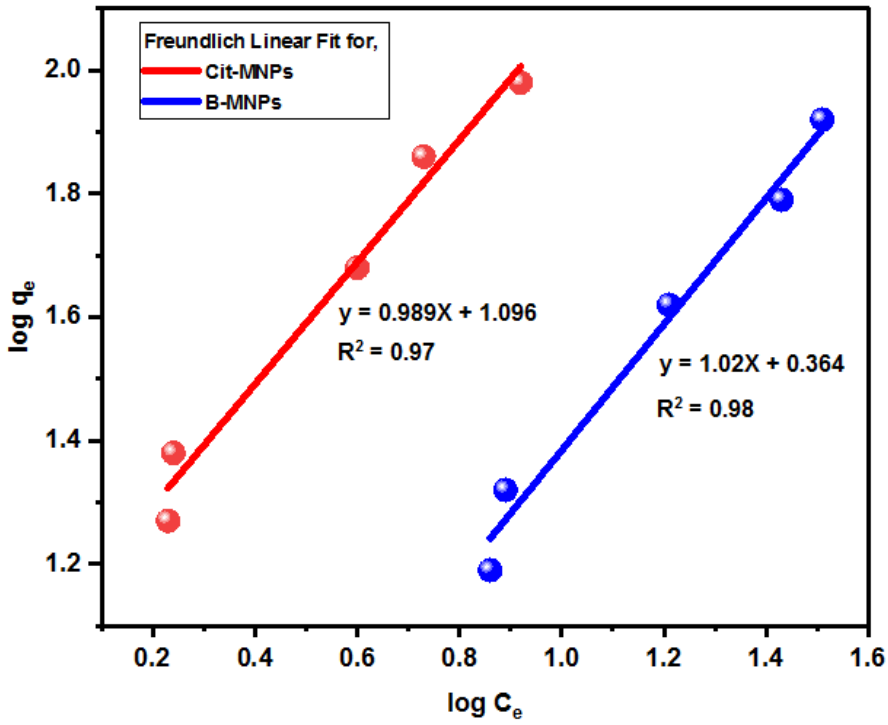

Figure 23. Fitting to Freundlich isotherm model for B-MNPs and Cit-MNPs

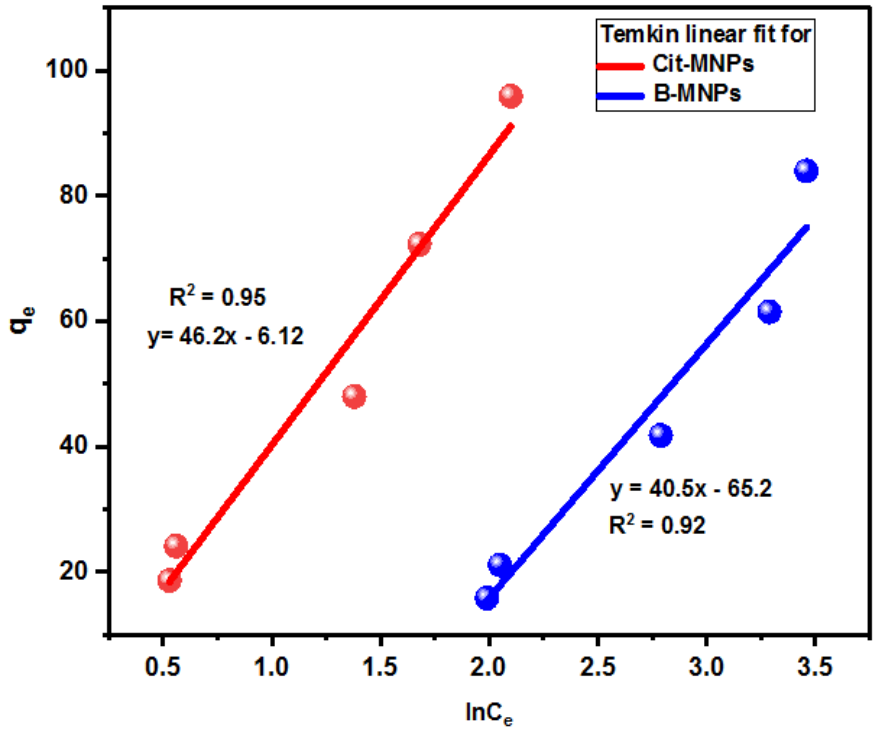

Figure 24. Fitting to Temkin adsorption isotherm for Cit-MNPs and B-MNPs

Table 4. The parameters extracted from isotherm models.

Adsorbent Sample	Isotherm Model									
	Langmuir parameters			Freundlich Parameter			Temkin parameters			
	q_{max} (mg/g)	B	R^2	n	1/n	K_f	R^2	B_T	K_T	R^2
B-MNPs	111.11	0.021	0.94	0.98	1.02	2.31	0.98	40.5	0.2	0.92
Cit-MNPs	200.00	0.06	0.94	1.011	0.98	12.47	0.97	46.2	0.9	0.95

Table 5. The parameters for plotting Langmuier, Freundlich, and Temkin adsorption Isotherms for Pb^{2+} onto B-MNPs and Cit-MNPs.

Adsorbent	Initial Con.	C_e(mg/g)	q_e(mg/g)	$1/C_e$	$1/q_e$	log C_e	Log q_e	lnC_e
B-MNPs	25	7.3	15.84	0.137	0.063	0.86	1.19	1.99
	50	7.75	21.13	0.129	0.047	0.89	1.32	2.05
	100	16.4	41.8	0.061	0.024	1.21	1.62	2.79
	150	27	61.5	0.037	0.016	1.43	1.79	3.29
	200	32	84	0.031	0.012	1.51	1.92	3.46
Cit-MNP	25	1.7	18.62	0.588	0.054	0.23	1.27	0.53
	50	1.75	24.13	0.571	0.041	0.24	1.38	0.56
	100	4.0	48.0	0.25	0.021	0.60	1.68	1.38
	150	5.4	72.3	0.185	0.014	0.73	1.86	1.68
	200	8.2	95.9	0.122	0.010	0.92	1.98	2.10

A comparison of the maximum adsorption capacity of different adsorbents obtained from the literature reviews summarized in Table 6.

Table 6. Comparison of maximum adsorption capacity of some selected adsorbents for Pb^{2+} ions.

Adsorbent material (Conventional Adsorbent)	Maximum adsorption Capacity	Reference
Activated carbon	109.9 mg/g	[38]
Peat moss	16.2 mg/g	[41]
Flay ash	6.0 mg/g	[40]
Clay	0.4 mg/g	[42]
Zeolite	57.5 mg/g	[43]
Humic acid coating magnetic nanoparticles	97.7 mg/g	[64]
MNPs mesoporous silica structure surface-modified with-SH organic groups	47.25 mg/g	[62]
Thiol functionalized magnetite mesoporous	206 mg/g	[60]
Magnetic chitosan resin modified with thiourea	261.6 mg/g	[65]
Amino-functionalized $Fe_3O_4@SiO_2$ MNPs with a core-shell structure	108.9 mg/g	[59]
Magnetite modified with succinic acid, ethylenediamine and 2, 3-dimercaptosuccinic acid groups.	135.6 mg/g	[57]
Bare magnetite nanoadsorbent (B-MNPs)	111.1 mg/g	This work
Citric acid-modified nanoadsorbent (Cit-MNPs)	200.0 mg/g	This work

4.5 Modeling of adsorption kinetics

The kinetic studies of adsorption experiments are highly significant and important to classify the rate of sorption, reaction path, adsorbent efficiency, and system reaction rate [70]. The kinetic evaluations of the adsorptions of Pb^{2+} ions onto magnetite nanoadsorbents have been performed by fitting the equilibrium sorption data into the well known Lagergren's pseudo-first-order and pseudo-second-order kinetic models [77].

Based on the given data in Table 7, pseudo-first-order and pseudo-second-order kinetic models were plotted. For further information, see Appendix B.

Figures (25 and 26), described the pseudo first and pseudo second order model of B-MNPs and Cit-MNPs accompanied with R^2 value.

As listed in Table 8, comparatively, the big difference between $q_{e,exp}$ and $q_{e,cal}$ from Pseudo first-order kinetic models showed that the adsorptions of Pb^{2+} ions onto B-MNPs do not obey pseudo-first-order kinetics. And also based on the values of the correlation coefficient (R^2), the pseudo-first-order kinetic equation for B-MNPs was not applicable because the value of R^2 obtained is very small, around $R^2 = 0.55$. However, the $q_{e,cal}$ values obtained through pseudo-second-order models are almost closer to the experimental $q_{e,exp}$ values. Moreover, the pseudo-second-order kinetics model indicated a higher correlation coefficient, around $R^2 = 0.99$. Therefore, in the case of B-MNPs, the correlation coefficients and theoretical q_e values obtained for the pseudo-second-order kinetic models are preferred over the pseudo-first-order. Hence, the adsorption methods follow the pseudo-second-order kinetic model that considers chemisorption. The reason may be that the presence of hydroxyl (OH^-) groups on the surface of B-MNPs due to deprotonation at optimized (pH 5) enhances chemical interaction with Pb^{2+} ions.

In addition, from (Figures 25 and 26), the sorption data was further applied to the case of Cit-MNPs. Careful evaluation of the kinetic data cleared that the equilibrium sorption data showed a better fit to pseudo-second-order model as compared to that of the pseudo-first-order. Nearly closer quantity of q_e values are obtained between the theoretically ($q_{e,cal}$ = 24.39 mg/L) and experimentally ($q_{e,exp}$ = 24.01 mg/L) for pseudo-second-order model. The fact is well supported by the high values of the correlation coefficient of R^2 = 0.99 as compared to that obtained by pseudo-first-model (R^2) = 0.48 for Cit-MNPs. The calculated variables justify that the sorption of Pb^{2+} ions onto the surface of magnetic nanoadsorbent is mainly administered by a chemisorption mechanism. The chemical interaction among carboxyl functional groups of the CA on nanoadsorbents and Pb^{2+} ions facilitated the rate of sorption. A similar kinetic trend was also reported by M.A. Atieh, et al. [76].

Table 7. Parameters for plotting adsorption of pseudo-first and pseudo-second-order.

Adsorbent	Time (min)	q_e (mg/g)	q_t(mg/g)	$q_e - q_t$	$\log(q_e - q_t)$	t/q_t
	20	20.88	16.74	4.14	0.617	1.195
	40	20.88	19.98	0.9	-0.046	2.00
	60	20.88	20.88	0	-	2.87
	80	20.88	20.69	0.19	-0.721	3.87
B-MNPs	120	20.88	20.58	0.3	-0.523	5.83
	20	24.01	20.08	3.93	0.59	0.996
	40	24.01	24.01	0.0	-	1.666
	60	24.01	23.91	0.1	-1	2.51
	80	24.01	23.99	0.02	-1.699	3.33
Cit-MNPs	120	24.01	23.96	0.05	-1.3	5.01

Table 8. Calculated parameters from the two kinetic models for B-MNPs and Cit- MNPs.

		Pseudo-first-order			Pseudo-second-order		
Adsorbent	$Q_{e,exp}$	$Q_{e,cal}$	$K_1(min^{-1})$	R^2	$Q_{e,cal}$	$K_2(min^{-1})$	R^2
B-MNPs	20.88	3.67	0.011	0.55	21.28	0.013	0.99
Cit-MNPs	24.01	3.26	0.019	0.48	24.39	0.014	0.99

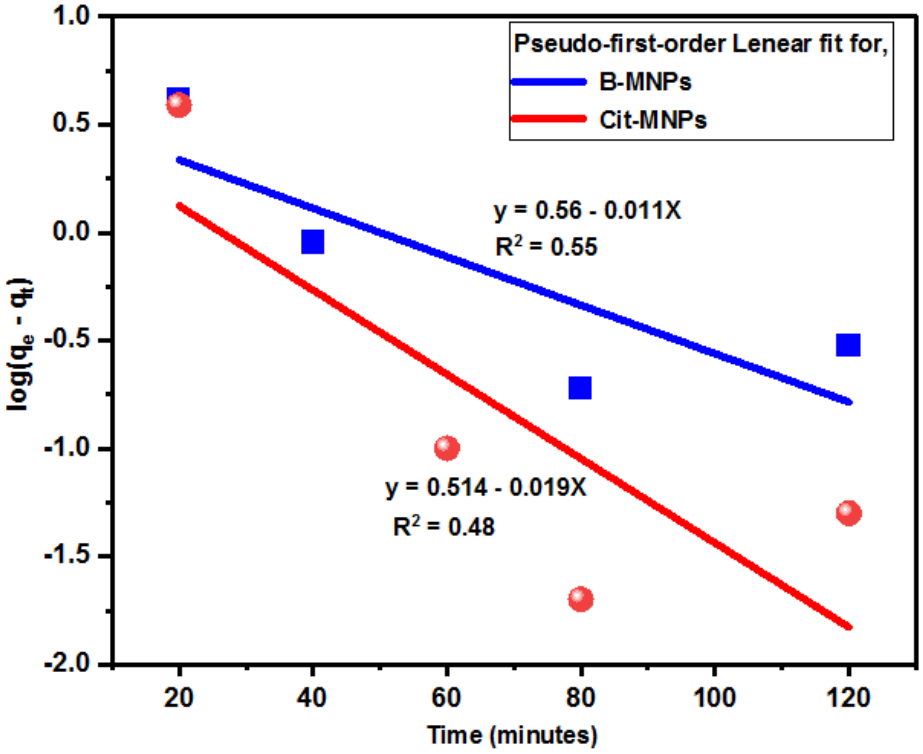

Figure 25. Fitting to Pseudo-first-order kinetic model for B-MNPs and Cit-MNPs

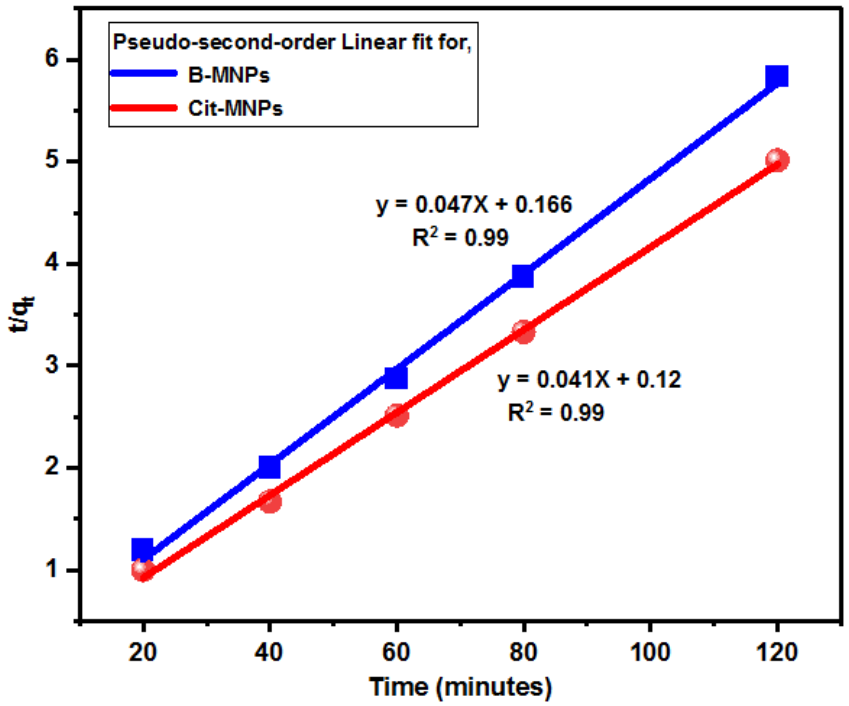

Figure 26. Fitting to Pseudo-second-order kinetic models for B-MNPs and Cit- MNPs

4. 6 Desorption and reusability studies

4.6.1 Desorption process of Pb^{2+} ions

Desorption is useful for the recovery of metal ions and to regenerate the exhausted nanoadsorbents. Desorption studies were conducted to select the optimum desorbing agent and to determine the number of successive regeneration cycles. The hydroxyl and carboxylic groups on the MNPs surface made it easy for desorption and regeneration with the acid solutions [78].

Three different desorption eluents, such as de-ionized water, HCl and HNO_3, were used to desorb Pb^{2+} ions from MNPs. To select the optimum desorption agent, experiments were conducted with 0.1 g/L of lead-loaded nanoadsorbents (B-MNPs and Cit-MNPs) agitated with 60 mL of 0.2 M concentration eluents at lower pH 2 and shaken on the rotary shaker for 1 hour at 200 rpm of a normal temperature in three replicates and taken the mean value. The percentage desorption of Pb^{2+} ions was calculated using the formula below (E. Katsou et al.) [79]

$$\text{Percentage of desorption} = \frac{\text{Concentration of Metal Desorbed}}{\text{Concentration of Metal Adsorbed}} \text{ X } 100, \quad \ldots\ldots\ldots\ldots \quad (17)$$

HCl and HNO_3 eluents recovered about 96.7% and 90.0% of Pb^{2+} adsorbed on the Cit-MNPs surface, respectively (Table 9 and Figure 27). Similarly, HCl and HNO_3 also desorbed (recover) 97.3% and 93.4% of the Pb^{2+} ions adsorbed on B-MNPs, respectively. But, de-ionized water showed low (insignificant) desorption percentages of 9.5% and 10.4% for Cit-MNPs and B-MNPs, respectively. Therefore, in this study, 0.2 M HCl eluent solutions were selected as desorption reagents for removing Pb^{2+} ions from the MNPs adsorbents. Hydrochloric acid (HCl) is commonly applied as the elution agent of metal ions, including Pb^{2+} ions, from sorbents due to their high solubility, commonly used in industry, and its relatively low cost (Naja and Volesky) [80].

Table 9. Optimizing desorbing efficiency of Pb2+ by different eluents in three replicates.

Nano adsorbent	B-MNPs								
Eluents	de-ionized water			HCl			HNO3		
	Adsorbed Conc. (C_{ad})	Desorbed Conc. (C_{de})	De-sorption (%)	Adsorbed Conc. (C_{ad})	Desorbed Conc. (C_{de})	De-sorption (%)	Adsorbed Conc. (C_{ad})	De-sorbed Conc. (C_{de})	De-sorption (%)
Replicate1	33.98	3.60	10.6%	34.11	33.41	98%	33.89	32.12	94.8%
Replicate2	34.02	3.54	10.4%	33.91	32.96	97.2%	33.78	31.55	93.4%
Replicate3	33.87	3.45	10.2%	33.99	32.90	96.8%	34.16	31.67	92.7%
Average	33.96	3.53	10.4%	34.00	33.09	97.3%	33.94	31.78	93.4%
Nano-adsorbent	Cit-MNPs								
Replicate1	48.32	4.59	9.5%	47.77	45.81	95.9%	48.04	43.04	89.6%
Replicate2	47.98	4.70	9.8%	48.92	47.79	97.7%	47.83	43.38	90.7%
Replicate3	48.67	4.48	9.2%	48.11	46.42	96.5%	48.22	43.25	89.7%
Average	48.32	4.59	9.5%	48.27	46.67	96.7%	48.03	43.22	90.0%

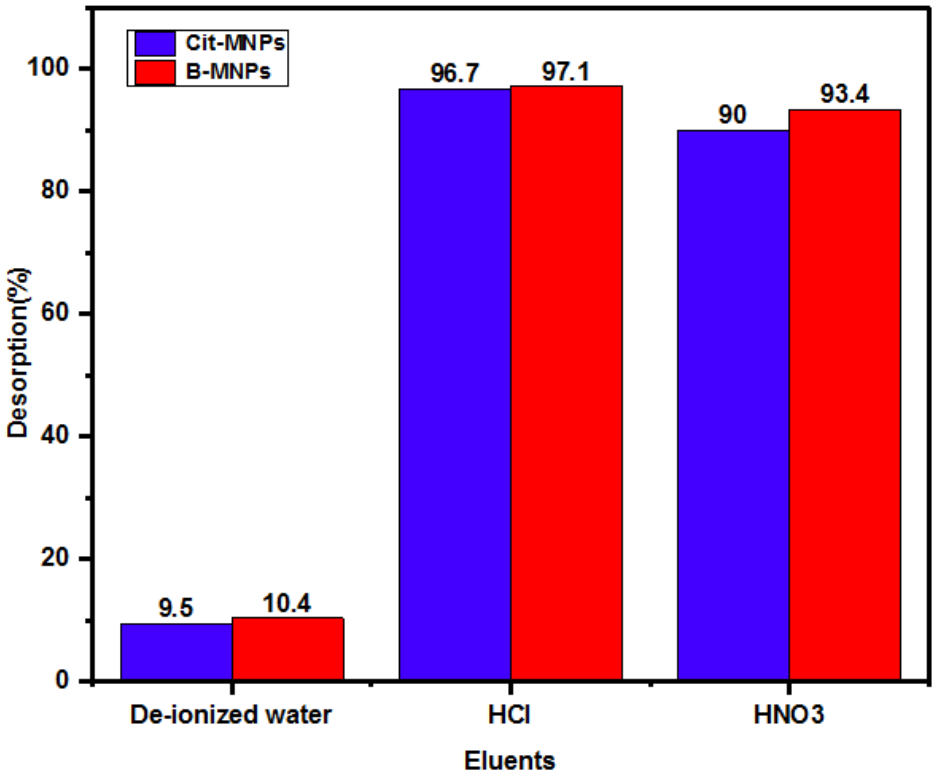

Figure 27. Desorption efficiency of different eluents (volume 60 ml; concentration = 0.2 M; pH 2; 200 rpm)

4.6.2 Reusability of MNPs

The reusability of used MNPs was investigated by performing five consecutive adsorption-desorption-regeneration cycles. For each cycle, the nanoadsorbents (B-MNPs and Cit-MNPs) mixed with 50 mL in the volume of 50 mg/L, 100 mg/L and 150 mg/L Pb^{2+} ion concentrations to evaluate the reusability efficiency of synthesized NPs. The desorption of the Fe_3O_4 nanoadsorbents containing Pb^{2+} ions was carried out in 60 mL of 0.2 M HCl and shaken on an orbital shaker for 1 hour at 200 rpm in room temperature conditions. The MNPs were then separated using a magnet from the desorbent solution. AAS was used to determine the concentration of Pb^{2+} ions in the supernatant solution. The magnetically recovered NPs were washed three times with de-ionized water. Then, the washed nanoadsorbents were dried in an electric, hot air oven at 80 $^{\circ}$C for 24 hours and reused for the subsequent adsorption cycle.

(Figure 28) illustrated that during adsorption-desorption-regeneration processes the percentage removal efficiency of B-MNPs for 50 mg/L, 100 mg/L and 150 mg/L Pb^{2+} ion concentrations were (84.5, 81.7, 78.5, 73.2, and 62%), (83.6, 81.4, 77.3, 70.9, and 57.3%), and (82, 79.1, 75, 68.4, and 56.1%), for the first, second, third, fourth, and fifth cycles, respectively

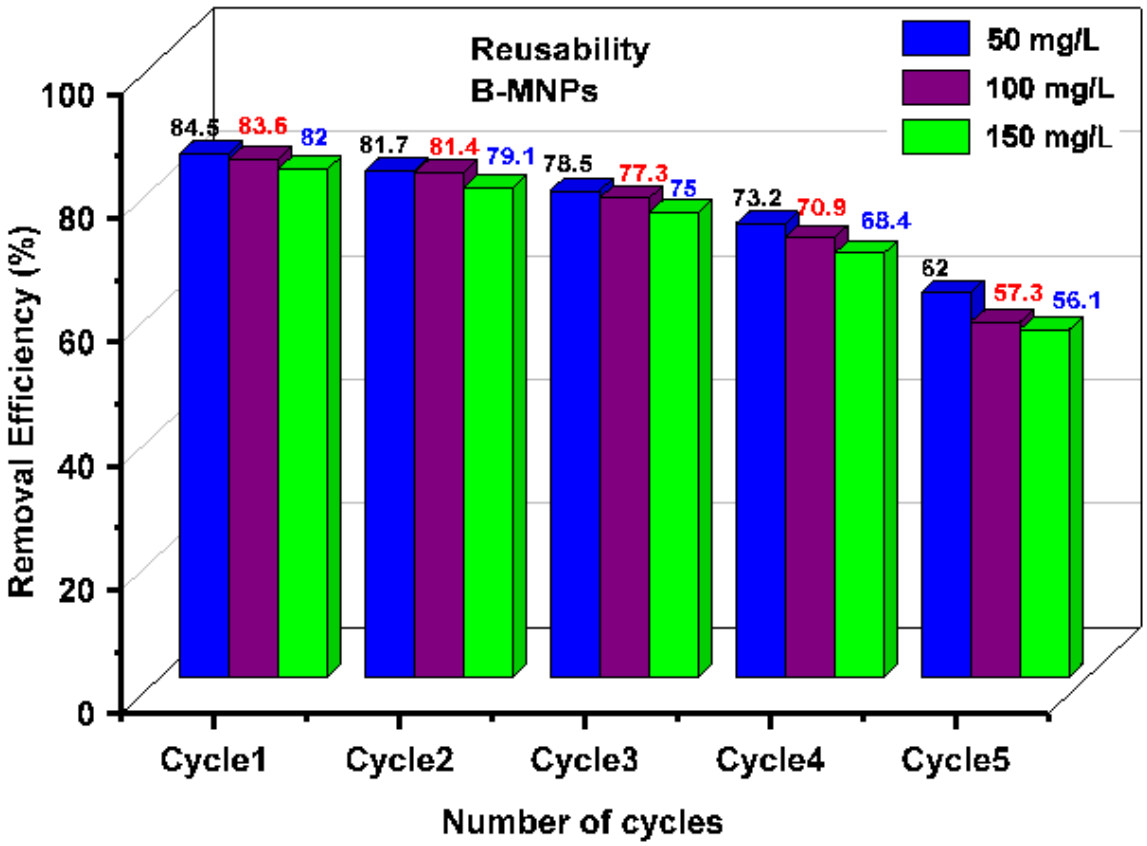

Figure 28. Reusability study of B-MNPs during 5 cycle (initial Pb^{2+} concentration = 50, 100,150 mg/L; adsorbent doze = 0.1 g/L; pH 5; contact time = 1 hour, rpm = 200).

In the case of Cit-MNPs (Figure 29), the results showed that the percentage removal efficiency of Pb^{2+} ions from the solution with the same concentration (50, 100, and 150 mg/L) in the respective five cycles of adsorption-desorption processes were (96.5, 94, 91.5, 88.2, and 64.5%), (96, 92.8, 89.9, 85.9, and 62.8%), and (96.4, 93.9, 91.4, 87.6, and 61.6%), respectively. From the results, it was observed that the adsorption efficiency of as-synthesized MNPs slightly decreased from the first cycle up to the fourth cycle of adsorption-desorption-regeneration process. While, in the fifth cycle, removal efficiency

was highly decreased due to functional groups on the surface of MNPs getting slacked after each adsorption-desorption processes. The removal efficiency greater than 50% after the fourth cycle means that the MNPs can be reused repeatedly and sustainable for the removal of Pb^{2+} ions. This is an important characteristic of a good adsorbent (Ramana et al., 2013).

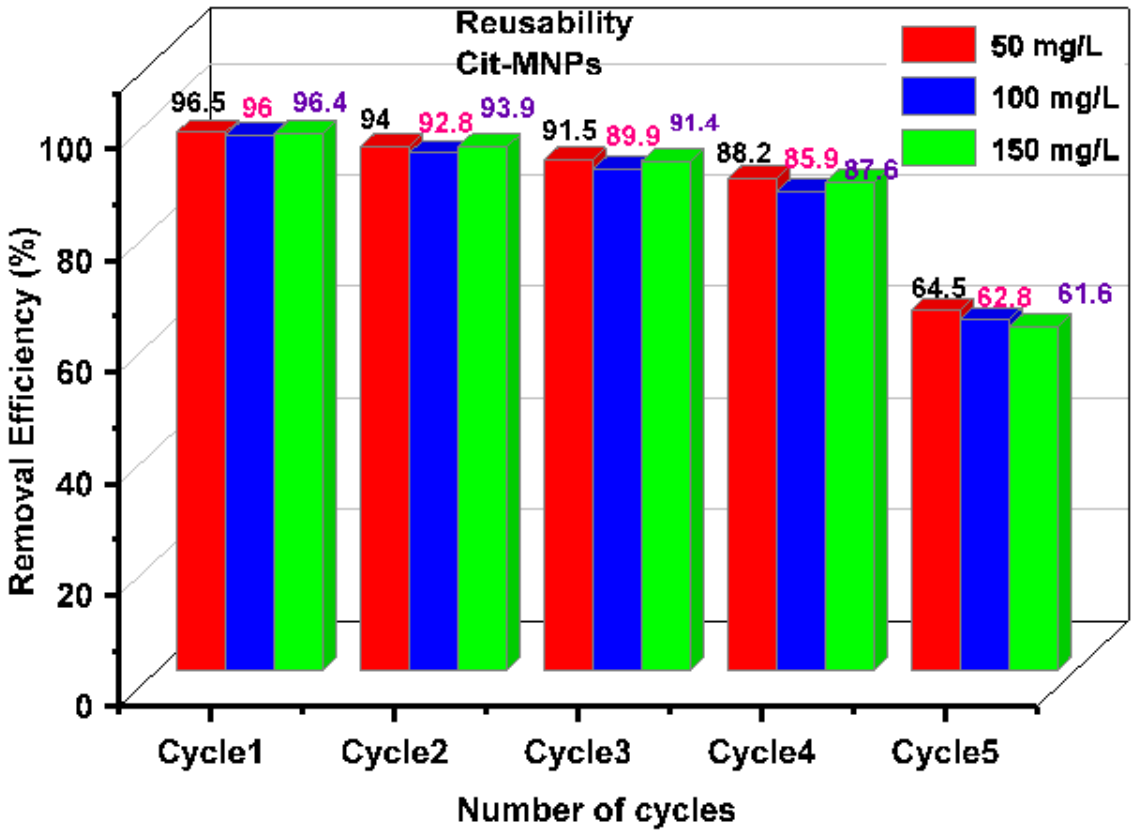

Figure 29. Reusability study of Cit-MNPs during 5 cycle (initial Pb^{2+} concentration = 150 mg/L, adsorbent = 0.1 g/L, pH 5, contact time = 1 hour, rpm = 200).

CHAPTER FIVE

Conclusions and Recommendations

5.1 Conclusions

The thesis work aimed to evaluate and compare the adsorbing efficiencies of B-MNPs and Cit-MNPs for the removal of heavy metal Pb^{2+} ions from synthetic wastewater through the batch adsorption process. The magnetite (Fe_3O_4) was prepared via conventional co-precipitation techniques. CA surface coatings were applied during the in-situ preparation of nanoparticles for functionalization with COOH groups. Surface modification of Fe_3O_4 with these specific organic functional groups was performed to enhance the selectivity of the MNPs towards Pb^{2+} ions. The XRD characterization of the prepared sample results confirmed that peaks of the nano-crystalline MNPs matched well with standard JCPDs file to Fe_3O_4.The approximated crystallite size of MNPs prepared through the co-precipitation method was calculated by the Scherrer formula and found to be 62.4 nm in diameter.

To avoid possible aggregation occurring, Fe_3O_4 were coated and functionalized with CA. The carboxyl group bound MNPs allowed particles to have high stability in an aqueous medium. Therefore, particle aggregation, and sedimentation did not occur. FTIR results confirmed the presence of COO^-, OH^-, and C-O groups on the surface of Fe_3O_4 NPs. Therefore, this indicated that CA are attached and bind to the MNPs. From zetasizer potential measurements, it was confirmed that the synthesized powder samples are in the nanometer scale range, around 82.14 ± 0.52 nm in diameter. It also had been observed that, adsorption of CA onto the surface of MNPs results in highly negative surface charges. This high negative value of zetapotential for the Cit-MNPs further confirmed the presence of carboxyl groups on the surface of MNPs, which facilitates sequestration of Pb^{2+} ions from wastewater by forming a chelating complex.

The maximum adsorption capacity of B-MNPs and Cit-MNPs was 111.1 mg/g and 200 mg/g, respectively, when 0.1 g/L adsorbents were used, at optimized pH 5, in 50 mg/L Pb^{2+} ions concentration, agitated at 200 rpm for 60 minutes, at ordinary temperature.

The Freundlich isotherm is the correct equation to express the Pb^{2+} ions uptake onto B-MNPs and Cit-MNPs. The removal efficiency of Pb^{2+} ions was recorded 83.5% and 96.3% by using B-MNPs and Cit-MNPs, respectively. Moreover, the adsorption kinetics models were best fitted with pseudo-second-order kinetics, which confirmed chemisorption. The desorption and recovery study showed that as-synthesized MNPs could be used repeatedly with the minor influence on the adsorption capacity.

5.2 Recommendations

For future works, the followings are recommended:

- Further study is recommended to investigate the removal capacity of functionalized magnetite nanoparticles towards other toxic heavy metals such as mercury, chromium, arsenic, zinc, etc. These toxic heavy metals can be found in manufacturing effluent such as leather and textile industries that may be carcinogenic to human health.

- The proposed magnetite nanoparticles were applied to determine their adsorbing removal efficiency onto artificially prepared (synthetic) wastewater. Further investigations into real wastewater (effluents from the industries) need to be made to understand its practical applications.

- The economic feasibility study is recommended for the application of these modified magnetite nanoparticles for the removal of Pb^{2+} ions from industrial wastewater.

References

[1] S. Bayda, M. Adeel, T. Tuccinardi, M. Cordani, and F. Rizzolio, "The history of nanoscience and nanotechnology: From chemical-physical applications to nanomedicine," Molecules, vol. 25, no. 1. 2020, doi: 10.3390/molecules25010112.

[2] F. Assa et al., "A biotechnological perspective on the application of iron oxide nanoparticles," Nano Research, vol. 9, no. 8. 2016, doi: 10.1007/s12274-016-1131-9.

[3] Y. Xia, Y. Xiong, B. Lim, and S. E. Skrabalak, "Shape-controlled synthesis of metal nanocrystals: Simple chemistry meets complex physics?" *AngewandteChemie - International Edition*, vol. 48, no. 1. 2009, doi: 10.1002/anie.200802248.

[4] S. I. Ohkoshi and H. Tokoro, "Hard magnetic ferrite: ε-Fe2O3," *Bull. Chem. Soc. Jpn.*, vol. 86, no. 8, 2013, doi: 10.1246/bcsj.20130120.

[5] C. N. Lininger et al., "Energetics of Lithium Insertion into Magnetite, Defective Magnetite, and Maghemite," Chem. Mater., vol. 30, no. 21, 2018, doi: 10.1021/acs.chemmater.8b03544.

[6] C. Das et al., "Green synthesis, characterization and application of natural product coated magnetite nanoparticles for wastewater treatment," Nanomaterials, vol. 10, no. 8, 2020, doi: 10.3390/nano10081615.

[7] L. Shen, B. Li, and Y. Qiao, "Fe_3O_4 nanoparticles in targeted drug/gene delivery systems," *Materials*, vol. 11, no. 2. 2018, doi: 10.3390/ma11020324.

[8] H. Ali, E. Khan, and I. Ilahi, "Environmental chemistry and ecotoxicology of hazardous heavy metals: Environmental persistence, toxicity, and bioaccumulation," Journal of Chemistry, vol. 2019. 2019, doi: 10.1155/2019/6730305.

[9] WHO, "Guidelines for Drinking-water Quality: Third edition, incorporating the first and second Addenda, Volume 1 Recommendations," *World Heal. Organ.*, vol. 1, 2008.

[10] O. Plohl, M. Simonič, K. Kolar, S. Gyergyek, and L. Fras Zemljič, "Magnetic nanostructures functionalized with a derived lysine coating applied to simultaneously remove heavy metal pollutants from environmental systems," *Sci. Technol. Adv. Mater.*, vol. 22, no. 1, 2021, doi: 10.1080/14686996.2020.1865114.

[11] A. Goodarzi, Y. Sahoo, M. T. Swihart, and P. N. Prasad, "Aqueous ferrofluid of citric acid coated magnetite particles," in *Materials Research Society Symposium - Proceedings*, 2003, vol. 789, doi: 10.1557/proc-789-n6.6.

[12] E. Cheraghipour, S. Javadpour, and A. R. Mehdizadeh, "Citrate capped superparamagnetic iron oxide nanoparticles used for hyperthermia therapy," *J. Biomed. Sci. Eng.*, vol. 05, no. 12, 2012, doi: 10.4236/jbise.2012.512089.

[13] K. Singh, N. A. Renu, and M. Agarwal, "Methodologies for removal of heavy metal ions from wastewater: an overview," *Interdiscip. Environ. Rev.*, vol. 18, no. 2, 2017, doi: 10.1504/ier.2017.10008828.

[14] E. Cheraghipour, A. M. Tamaddon, S. Javadpour, and I. J. Bruce, "PEG conjugated citrate-capped magnetite nanoparticles for biomedical applications," *J. Magn.Magn.Mater.*, vol. 328, 2013, doi: 10.1016/j.jmmm.2012.09.042.

[15] S. Gopalakrishnan, A. Sathya, R. Vijayabharathi, R. K. Varshney, C. L. L. Gowda, and L. Krishnamurthy, "Plant growth promoting rhizobia: challenges and opportunities," *3 Biotech*, vol. 5, no. 4. 2015, doi: 10.1007/s13205-014-0241-x.

[16] M. Jaishankar, T. Tseten, N. Anbalagan, B. B. Mathew, and K. N. Beeregowda, "Toxicity, mechanism and health effects of some heavy metals," *Interdisciplinary Toxicology*, vol. 7, no. 2. 2014, doi: 10.2478/intox-2014-0009.

[17] Global Health Observatory: on lead paint, Geneva: World Health Organization; 2021)

[18] P. B. Tchounwou, C. G. Yedjou, A. K. Patlolla, and D. J. Sutton, "Heavy metal toxicity and the environment," *EXS*, vol. 101. 2012, doi: 10.1007/978-3-7643-8340-4_6.

[19] V.Masindi and K. L. Muedi, "Environmental Contamination by Heavy Metals, Heavy Metals, June 27th 2018. Available from: https://www.intechopen.com/chapters/60680

[20] N. Tananaev, R. Teisserenc, and M. Debolskiy, "Permafrost hydrology research domain: Process-based adjustment," *Hydrology*, vol. 7, no. 1, 2020, doi: 10.3390/hydrology7010006.

[21] M. Balali-Mood, K. Naseri, Z. Tahergorabi, M. R. Khazdair, and M. Sadeghi, "Toxic Mechanisms of Five Heavy Metals: Mercury, Lead, Chromium, Cadmium, and Arsenic," *Frontiers in Pharmacology*, vol. 12. 2021, doi: 10.3389/fphar.2021.643972.

[22] M. Mohammad Ali, D. Hossain, Al-Imran, M. Suzan Khan, M. Begum, and M. Hasan Osman, "Environmental Pollution with Heavy Metals: A Public Health Concern," in *Heavy Metals - Their Environmental Impacts and Mitigation*, 2021.

[23] G. K. Kinuthia, V. Ngure, D. Beti, R. Lugalia, A. Wangila, and L. Kamau, "Levels of heavy metals in wastewater and soil samples from open drainage channels in Nairobi, Kenya: community health implication," *Sci. Rep.*, vol. 10, no. 1, 2020, doi: 10.1038/s41598-020-65359-5.

[24] EPA, Treatment technologies for Lead in soil, waste and water, remediation and technology innovation. Washington, DC, 2007

[25] A. Chiavola, S. Bongirolami, and G. Di Francesco, "Technical-economic comparison of chemical precipitation and ion exchange processes for the removal of phosphorus from wastewater," *Water Sci. Technol.*, vol. 81, no. 7, 2020, doi: 10.2166/wst.2020.023.

[26] H. Koren and M. S. Bisesi, "Solid and Hazardous Waste Management," in *Handbook of Environmental Health, Volume II*, 2020.

[27] F. Fu and Q. Wang, "Removal of heavy metal ions from wastewaters: A review," *Journal of Environmental Management*, vol. 92, no. 3. 2011, doi: 10.1016/j.jenvman.2010.11.011.

[28] N. A. A. Qasem, R. H. Mohammed, and D. U. Lawal, "Removal of heavy metal ions from wastewater: a comprehensive and critical review," *npj Clean Water*, vol. 4, no. 1. 2021, doi: 10.1038/s41545-021-00127-0.

[29] S. Sharma and A. Bhattacharya, "Drinking water contamination and treatment techniques," *Appl. Water Sci.*, vol. 7, no. 3, 2017, doi: 10.1007/s13201-016-0455-7.

[30] E. O. Ezugbe and S. Rathilal, "Membrane technologies in wastewater treatment: A review," *Membranes*, vol. 10, no. 5. 2020, doi: 10.3390/membranes10050089.

[31] C. M. Narayanan and V. Narayan, "Biological wastewater treatment and bioreactor design: A review," *Sustainable Environment Research*, vol. 1, no. 1. 2019, doi: 10.1186/s42834-019-0036-1.

[32] Y. Hua, J. Xiao, Q. Zhang, C. Cui, and C. Wang, "Facile synthesis of surface-functionalized magnetic nanocomposites for effectively selective adsorption of cationic dyes," *Nanoscale Res. Lett.*, vol. 13, 2018, doi: 10.1186/s11671-018-2476-7.

[33] S. De Gisi, G. Lofrano, M. Grassi, and M. Notarnicola, "Characteristics and adsorption capacities of low-cost sorbents for wastewater treatment: A review," *Sustainable Materials and Technologies*, vol. 9. 2016, doi: 10.1016/j.susmat.2016.06.002.

[34] O. Hakami, Y. Zhang, and C. J. Banks, "Thiol-functionalisedmesoporous silica-coated magnetite nanoparticles for high efficiency removal and recovery of Hg from water," *Water Res.*, vol. 46, no. 12, 2012, doi: 10.1016/j.watres.2012.04.032.

[35] P. O. Bedolla*et al.*, "Effects of van der Waals interactions in the adsorption of isooctane and ethanol on Fe(100) surfaces," *J. Phys. Chem. C*, vol. 118, no. 31, 2014, doi: 10.1021/jp503829c

[36] P. O. Oladoye, "Natural, low-cost adsorbents for toxic Pb(II) ion sequestration from (waste)water: A state-of-the-art review," *Chemosphere*, vol. 287. 2022, doi: 10.1016/j.chemosphere.2021.132130.

[37] J. Jjagwe, P. W. Olupot, E. Menya, and H. M. Kalibbala, "Synthesis and Application of Granular Activated Carbon from Biomass Waste Materials for Water Treatment: A Review," *Journal of Bioresources and Bioproducts*, vol. 6, no. 4. 2021, doi: 10.1016/j.jobab.2021.03.003.

[38] S. Kumar *et al.*, "Challenges and opportunities associated with waste management in India," *Royal Society Open Science*, vol. 4, no. 3. 2017, doi: 10.1098/rsos. 160764.

[39] U. O. Aigbe, K. E. Ukhurebor, R. B. Onyancha, O. A. Osibote, H. Darmokoesoemo, and H. S. Kusuma, "Fly ash-based adsorbent for adsorption of heavy metals and dyes from aqueous solution: a review," *Journal of Materials Research and Technology*, vol. 14. 2021, doi: 10.1016/j.jmrt.2021.07.140.

[40] A. Tripathi and M. RawatRanjan, "Heavy Metal Removal from Wastewater Using Low Cost Adsorbents," *J. Bioremediation Biodegrad.*, vol. 06, no. 06, 2015, doi: 10.4172/2155-6199.1000315.

[41] A. A. Adeyemo, I. O. Adeoye, and O. S. Bello, "Adsorption of dyes using different types of clay: a review," *Appl. Water Sci.*, vol. 7, no. 2, 2017, doi:10.1007/s13201-015-0322-y.

[42] J. Shi *et al.*, "Preparation and application of modified zeolites as adsorbents in wastewater treatment," *Water Sci. Technol.*, vol. 2017, no. 3, 2017, doi: 10.2166/wst.2018.249.

[43] M. Anjum, R. Miandad, M. Waqas, F. Gehany, and M. A. Barakat, "Remediation of wastewater using various nano-materials," *Arabian Journal of Chemistry*, vol. 12, no. 8. 2019, doi: 10.1016/j.arabjc.2016.10.004.

[44] S. Li, W. Wang, F. Liang, and W. X. Zhang, "Heavy metal removal using nanoscale zero-valent iron (nZVI): Theory and application," *J. Hazard. Mater.*, vol. 322, 2017, doi: 10.1016/j.jhazmat.2016.01.032.

[45] W. Wu, X. Xiao, S. Zhang, F. Ren, and C. Jiang, "Facile method to synthesize magnetic iron oxides/TiO 2 hybrid nanoparticles and their photodegradation application of methylene blue," *Nanoscale Res. Lett.*, vol. 6, 2011, doi: 10.1186/1556-276X-6-533.

[46] Z. Xu and J. Dong, "Synthesis, characterization, and application of magnetic nanocomposites for the removal of heavy metals from industrial effluents," in *Emerging Environmental Technologies*, 2008.

[47] J. Aguado, J. M. Arsuaga, A. Arencibia, M. Lindo, and V. Gascón, "Aqueous heavy metals removal by adsorption on amine-functionalized mesoporous silica," *J. Hazard.Mater.*, vol. 163, no. 1, 2009, doi: 10.1016/j.jhazmat.2008.06.080.

[48] C. Huang and B. Hu, "Silica-coated magnetic nanoparticles modified with γ-mercaptopropyltrimethoxysilane for fast and selective solid phase extraction of trace amounts of Cd, Cu, Hg, and Pb in environmental and biological samples prior to their determination by inductively coupled plasma mass spectrometry," *Spectrochim. Acta - Part B At.Spectrosc.*, vol. 63, no. 3, 2008, doi: 10.1016/j.sab.2007.12.010.

[49] J. Hu, G. Chen, and I. M. C. Lo, "Removal and recovery of Cr(VI) from wastewater by maghemite nanoparticles," *Water Res.*, vol. 39, no. 18, 2005, doi: 10.1016/j.watres.2005.05.051.

[50] J. T. Mayo *et al.*, "The effect of nanocrystalline magnetite size on arsenic removal," *Sci. Technol. Adv. Mater.*, vol. 8, no. 1–2, 2007, doi: 10.1016/j.stam.2006.10.005.

[51] S. Yean *et al.*, "Effect of magnetite particle size on adsorption and desorption of arsenite and arsenate," *J. Mater. Res.*, vol. 20, no. 12, 2005, doi: 10.1557/jmr.2005.0403.

[52] T. Tuutijärvi, J. Lu, M. Sillanpää, and G. Chen, "As(V) adsorption on maghemite nanoparticles," *J. Hazard. Mater.*, vol. 166, no. 2–3, 2009, doi: 10.1016/j.jhazmat.2008.12.069.

[53] M. A. Dheyab, A. A. Aziz, M. S. Jameel, O. A. Noqta, P. M. Khaniabadi, and B. Mehrdel, "Simple rapid stabilization method through citric acid modification for magnetite nanoparticles," *Sci. Rep.*, vol. 10, no. 1, 2020, doi: 10.1038/s41598-020-67869-8.

[54] B. Lesiak*et al.*, "Surface Study of Fe3O4 Nanoparticles Functionalized With Biocompatible Adsorbed Molecules," *Front. Chem.*, vol. 7, 2019, doi: 10.3389/fchem.2019.00642.

[55] B. Behdadfar, A. Kermanpur, H. Sadeghi-Aliabadi, M. D. P. Morales, and M. Mozaffari, "Synthesis of high intrinsic loss power aqueous ferrofluids of iron oxide nanoparticles by citric acid-assisted hydrothermal-reduction route," *J. Solid State Chem.*, vol. 187, 2012, doi: 10.1016/j.jssc.2011.12.011.

[56] P. N. Dave and L. V. Chopda, "Application of iron oxide nanomaterials for the removal of heavy metals," *Journal of Nanotechnology*, vol. 2014. 2014, doi: 10.1155/2014/398569.

[57] J. F. Liu, Z. S. Zhao, and G. Bin Jiang, "Coating Fe3O4 magnetic nanoparticles with humic acid for high efficient removal of heavy metals in water," *Environ. Sci. Technol.*, vol. 42, no. 18, 2008, doi: 10.1021/es800924c.

[58] C. Meng, W. Zhikun, L. Qiang, L. Chunling, S. Shuangqing, and H. Songqing, "Preparation of amino-functionalized Fe3O4@mSiO2 core-shell magnetic nanoparticles and their application for aqueous Fe3+ removal," *J. Hazard. Mater.*, vol. 341, 2018, doi: 10.1016/j.jhazmat.2017.07.062.

[59] J. Brown, R. Richer, and L. Mercier, "One-step synthesis of high capacity mesoporous Hg2+ adsorbents by non-ionic surfactant assembly," *MicroporousMesoporous Mater.*, vol. 37, no. 1–2, 2000, doi: 10.1016/S1387-1811(99)00191-2.

[60] J. Brown, L. Mercier, and T. J. Pinnavaia, "Selective adsorption of Hg2+ by thiol-functionalized nanoporous silica," *Chem. Commun.*, no. 1, 1999, doi: 10.1039/a807249c.

[61] S. V. Mattigod, G. E. Fryxell, and K. E. Parker, "A thiol-functionalized nanoporous silica sorbent for removal of mercury from actual industrial waste," in *Environmental Applications of Nanomaterials: Synthesis, Sorbents and Sensors*, 2007.

[62] H. Yoshitake, T. Yokoi, and T. Tatsumi, "Adsorption of chromate and arsenate by amino-functionalized MCM-41 and SBA-1," *Chem. Mater.*, vol. 14, no. 11, 2002, doi: 10.1021/cm0202355.

[63] A. M. Donia, A. A. Atia, and K. Z. Elwakeel, "Selective separation of mercury(II) using magnetic chitosan resin modified with Schiff's base derived from thiourea and

glutaraldehyde," *J. Hazard. Mater.*, vol. 151, no. 2–3, 2008, doi: 10.1016/j.jhazmat.2007.05.083.

[64] Suyanta*et al.*, "Superparamagneticnanocomposite of magnetite-chitosan using oleic acid as anti-agglomeration and glutaraldehyde as crosslinkage agent," *Indones. J. Chem.*, vol. 19, no. 1, 2019, doi: 10.22146/ijc.28989.

[65] P. Majewski and B. Thierry, "Critical Reviews in Solid State and Materials Sciences Functionalized Magnetite Nanoparticles-Synthesis, Properties, and Bio-Applications Functionalized Magnetite Nanoparticles-Synthesis, Properties, and Bio-Applications," *Crit. Rev. Solid State Mater. Sci.*, vol. 32, 2007.

[66] A. K. Bordbar, A. A. Rastegari, R. Amiri, E. Ranjbakhsh, M. Abbasi, and A. R. Khosropour, "Characterization of Modified Magnetite Nanoparticles for Albumin Immobilization," *Biotechnol. Res. Int.*, vol. 2014, 2014, doi: 10.1155/2014/705068.

[67] A. Qureashi, A. H. Pandith, A. Bashir, T. Manzoor, L. A. Malik, and F. A. Sheikh, "Citrate coated magnetite: A complete magneto dielectric, electrochemical and DFT study for detection and removal of heavy metal ions," *Surfaces and Interfaces*, vol. 23, 2021, doi: 10.1016/j.surfin.2021.101004.

[68] X. Liu, L. Xu, Y. Liu, and W. Zhou, "Synthesis of citric acid-modified resins and their adsorption properties towards metal ions," *R. Soc. Open Sci.*, vol. 5, no. 8, 2018, doi: 10.1098/rsos.171667.

[69] F. Batool, J. Akbar, S. Iqbal, S. Noreen, and S. N. A. Bukhari, "Study of Isothermal, Kinetic, and Thermodynamic Parameters for Adsorption of Cadmium: An Overview of Linear and Nonlinear Approach and Error Analysis," *Bioinorg. Chem. Appl.*, vol. 2018, 2018, doi: 10.1155/2018/3463724.

[70] E. Mekonnen, M. Yitbarek, and T. R. Soreta, "Kinetic and thermodynamic studies of the adsorption of Cr(VI) onto some selected local adsorbents," *South African J. Chem.*, vol. 68, 2015, doi: 10.17159/0379-4350/2015/v68a7.

[71] D. L. Dorset, "X-ray Diffraction: A Practical Approach," *Microsc. Microanal.*, vol. 4, no. 5, 1998, doi: 10.1017/S143192769800049X.

[72] K. M. Kim *et al.*, "Surface treatment of silica nanoparticles for stable and charge-controlled colloidal silica," *Int. J. Nanomedicine*, vol. 9, 2014, doi: 10.2147/IJN.S57922.

[73] M. M. Abutalib and A. Rajeh, “Influence of Fe3O4 nanoparticles on the optical, magnetic and electrical properties of PMMA/PEO composites: Combined FT-IR/DFT for electrochemical applications,” *J. Organomet. Chem.*, vol. 920, 2020, doi: 10.1016/j.jorganchem.2020.121348.

[74] E. Igberase, P. Osifo, and A. Ofomaja, “The Adsorption of Pb, Zn, Cu, Ni, and Cd by Modified Ligand in a Single Component Aqueous Solution: Equilibrium, Kinetic, Thermodynamic, and Desorption Studies,” *Int. J. Anal. Chem.*, vol. 2017, 2017, doi: 10.1155/2017/6150209.

[75] R. Bhateria and R. Singh, “A review on nanotechnological application of magnetic iron oxides for heavy metal removal,” *Journal of Water Process Engineering*, vol. 31. 2019, doi: 10.1016/j.jwpe.2019.100845.

[76] M. A. Atieh, O. Y. Bakather, B. Al-Tawbini, A. A. Bukhari, F. A. Abuilaiwi, and M. B. Fettouhi, “Effect of carboxylic functional group functionalized on carbon nanotubes surface on the removal of lead from water,” *Bioinorg. Chem. Appl.*, vol. 2010, 2010, doi: 10.1155/2010/603978.

[77] E. D. Revellame, D. L. Fortela, W. Sharp, R. Hernandez, and M. E. Zappi, “Adsorption kinetic modeling using pseudo-first order and pseudo-second order rate laws: A review,” *Cleaner Engineering and Technology*, vol. 1. 2020, doi: 10.1016/j.clet.2020.100032.

[78] J. Bayuo, M. A. Abukari, and K. B. Pelig-Ba, “Desorption of chromium (VI) and lead (II) ions and regeneration of the exhausted adsorbent,” *Appl. Water Sci.*, vol. 10, no. 7, 2020, doi: 10.1007/s13201-020-01250-y.

[79]E. Katsou, S. Malamis, M. Tzanoudaki, K. J. Haralambous, and M. Loizidou, “Regeneration of natural zeolite polluted by lead and zinc in wastewater treatment systems,” J. Hazard. Mater., vol. 189, no. 3, 2011, doi: 10.1016/j.jhazmat.2010.12. 061.

[80] G. M. Naja and B. Volesky, “Biosorption for Industrial Applications,” in Comprehensive Biotechnology, Second Edition, vol. 6, 2011.

[81] Zheng, H., Schenk, J., Xu, R. et al. “Surface Morphology and Structurl Evolution of Magnetite-Based Iron Ore Fines During the Oxidation”. Metal Mater Trans B 53, 1644 – 1660, (2022)

APPENDICES

Appendix A: Optimization of parameters

Appendix A.1. Effects of pH on adsorbing capacity and efficiency of Pb (II) ion by B-MNPs and Cit-MNPs at [initial Pb^{2+} concentrations, 50 mg/L; Adsorbent dose, 0.1 g; and contact time, 120 minutes]

Adsorbent	pH	Adsorption Capacity Q_e(ppm)	Adsorption Efficiency (%)
B-MNPs	2	2.5	10
	3	12.99	52
	4	16.24	65
	5	20.86	83.5
	6	20.86	83.5
	7	20.51	82.1
	8	21.5	87.4
	9	23.18	92.7
	10	24	96
	11	24.5	98
Cit-MNPs	2	14.74	59
	3	16.94	67.8
	4	18.78	75.2
	5	24.05	96.3
	6	23.88	95.6
	7	24.71	98.9
	8	24.9	99.7
	9	24.9	99.7
	10	24.95	99.8
	11	24.98	99.9

Appendix A.2. Effects of adsorbent dose on adsorbing capacity and efficiency of Pb (II) ion by B-MNPs and Cit-MNPs at [pH, 6; initial Pb^{2+}concentrations, 50 mg/L; and contact time, 120minutes]

Adsorbent	Adsorbent dose (g)	Adsorption Capcity (ppm)	Adsorption Efficiency (%)
B-MNPs	0.05	41.73	83.5
	0.1	20.73	83
	0.15	11.81	71
	0.2	7.75	62
Cit-MNPs	0.05	43.37	86.8
	0.1	24.16	96.7
	0.15	16.01	96.1
	0.2	12.02	96.3

Appendix A.3. Effects of initial metal concentration on adsorbing capacity and efficiency of Pb (II) ion by B-MNPs and Cit-MNPs at [pH 6; Adsorbent dose, 0.1 g; and contact time, 120 minutes]

Adsorbents	Pb^{2+}Concen-Tration	Adsorption Capacity Q_e(ppm)	Adsorption Efficiency (%)
B-MNPs	25	8.85	70.8
	50	21.13	84.5
	100	41.8	83.6
	150	61.5	82
	200	84	84
Cit-MNPs	25	11.65	93.2
	50	24.13	96.5
	100	48.0	96
	150	72.3	96.4
	200	95.9	95.9

Appendix A.4. Effects of contact time on adsorbing capacity and efficiency of Pb (II) ion by B-MNPs and Cit-MNPs at [pH, 6; initial Pb^{2+}concentrations, 50 mg/L; and adsorbent dose, 0.1 g]

Adsorbent	Contact Time (min)	Adsorption Capacity Q_e	Adsorption Efficiency (%)
B-MNPs	20	16.74	67
	40	19.98	80
	60	20.88	83.6
	80	20.69	82.8
	120	20.58	82.4
Cit-MNPs	20	20.08	80.4
	40	24.01	96.1
	60	23.91	95.7
	80	23.99	96
	120	23.96	95.9

Appendix B: AAS Sample analysis for Pb^{2+} ions

Appendix B.1. Calibration data of Pb^{2+} and working parameters of AAS. Calibration curves were applied to find out the concentration of Pb(II) ions in the sample solution by comparing it to a set of standard samples of 1, 2, 3, 4 ppm Pb^{2+} concentrations.

Date: November 5, 2021

AAS Analysis Result of Samples

Pb

Calibration data

Standard	Conc. (ppm)	Abs.
1	1	0.00284
2	2	0.00494
3	3	0.00776
4	4	0.01018

Energy = 71.5 PMT [V] = 298 1 = 283.3 nm Slit width = 1.2 nm
Lamp current = 3 mA Detection limit = 0.06 ppm

Instrument: Analytikjena Atomic Absorption Spectrophotometer
Model: ZEEnit 700P # 150ZJP1025 Tech: Flame
SW-Version: Aspcts LS 1.3.1.0RCI

Sample Analyzed by:

Name_____

Signature_____

Date_____

Approved by:

Name_____

Signature_____

Date_____

Appendix B.2 AAS Sample analysis for B-MNPs at different parameters

Data Date : November 5, 2021

No.	Sample	Conc. In ppm
	Std	49.96
Initial metal ions concentration		
1	B-MNP25	7.3
2	B-MNP50	7.75
3	B-MNP100	16.4
4	B-MNP150	27
5	B-MNP200	32
6	B-MNP pH2	44.96
7	B-MNP pH3	23.98
8	B-MNP pH4	17.48
9	B-MNP pH5	9.64
10	B-MNP pH6	8.24
11	B-MNP pH7	8.94
Mass of Adsorbent dose (g)		
12	B-MNP0.05	8.23
13	B-MNP0.1	8.49
14	B-MNP0.15	14.48
15	B-MNP0.2	18.98
Contact time T (Minutes)		
16	B-MNP T20	16.48
17	B-MNP T40	9.99
18	B-MNP T60	8.19
19	B-MNP T80	8.59
20	B-MNP T120	8.79

Adsorption(C_e) - Desorption(C_{ed}) Equilibrium Concentration For B-MNPs			
Initial metal ion (Pb^{2+}) Conc.(C_o)	No of cycles	Adsorption concentration C_e(in ppm)	Desorption concentration C_{ed}(in ppm)
50mg/L	Cycle 1	7.75	41.40
	Cycle 2	9.15	40.03
	Cycle 3	10.75	38.45
	Cycle 4	13.40	35.86
	Cycle 5	19	30.38
100mg/L	Cycle 1	16.4	81.92
	Cycle 2	18.6	79.77
	Cycle 3	22.7	75.75
	Cycle 4	29.1	69.48
	Cycle 5	42.7	56.15
150mg/L	Cycle 1	27	120.54
	Cycle 2	31.35	116.27
	Cycle 3	37.5	110.12
	Cycle 4	47.4	100.21
	Cycle 5	65.85	82.13

Sample Analyzed by:

Name_____

Signature_____

Date_____

Approved by:

Name_____

Signature_____

Date_____

Appendix B.3 AAS Sample analysis for Cit-MNPs at different parameters

Data Date: November 11, 2021

No.	Sample	Conc. In ppm
	Std	49.96
Initial metal ions concentration		
1	Cit-MNP25	1.7
2	Cit-MNP50	1.75
3	Cit-MNP100	4
4	Cit-MNP150	5.4
5	Cit-MNP200	8.2
6	Cit-MNP pH2	20.48
7	Cit-MNP pH3	16.08
8	Cit-MNP pH4	12.39
9	Cit-MNP pH5	1.84
10	Cit-MNP pH6	2.19
11	Cit-MNP pH7	0.55
Mass of adsorbent dose (g)		
12	Cit-MNP 0.05	6.59
13	Cit-MNP 0.1	1.64
14	Cit-MNP 0.15	1.94
15	Cit-MNP 0.2	1.85
Contac time T (minutes)		
16	Cit-MNP T20	9.79
17	Cit-MNP T 40	1.95
18	Cit-MNP T 60	2.15
19	Cit-MNP T 80	1.99
20	Cit-MNP T 120	2.04

Adsorption (C_e). – Desorption ($C_{ed.}$) Equilibrium Concentration For Cit-MNPs			
Initial metal ion (Pb^{2+}) Conc.(C_o)	No of cycles	Adsorption Conc. $C_{e.}$ (ppm)	Desorption Conc. $C_{ed.}$ (ppm)
50mg/L	Cycle 1	1.75	40.04
	Cycle 2	3.00	45.82
	Cycle 3	4.25	44.61
	Cycle 4	5.90	42.99
	Cycle 5	17.75	31.44
100mg/L	Cycle 1	4.00	93.60
	Cycle 2	7.20	90.48
	Cycle 3	10.10	87.65
	Cycle 4	14.10	83.75
	Cycle 5	37.20	61.23
150mg/L	Cycle 1	5.40	140.98
	Cycle 2	9.15	137.32
	Cycle 3	12.90	133.67
	Cycle 4	18.60	128.11
	Cycle 5	57.60	90.09

Sample Analyzed by: Approved by:

Name_____ Name_____

Signature_____ Signature_____

Date_____ Date_____